5

Simulation of Thoracic Impact Experiments Using THORAX V Computer Model

by

Sanford B. Roberts
School of Engineering and Applied Science
University of California, Los Angeles, USA

Introduction

The human thoracic skeleton is a complex structural system composed of a variety of interconnected force transmitting members. Each one is unique in its geometry, articulation with its neighboring member and intrinsic material properties. Collectively, they form a structural framework which plays a key role in protecting the thoracic viscera (heart, lungs, liver, spleen and great vessels) from injury as a consequence of externally applied forces. This framework consists of primary and secondary structural elements; namely, those which form the first line of resistance to deformation (ribs, sternum, vertebral column) and others (certain muscles, tendons, ligaments) which participate involuntarily only after finite distortion of the main framework has occurred.

Voluntary effects such as the closure of the glottis and tensioning of the abdominal wall can play a significant role in increasing the resistance of the chest wall to deformation. Under these conditions air cannot readily escape and the volume of the abdomen cannot increase, thereby increasing the apparent chest stiffness dramatically. On the other hand, if the glottis is opened and the stomach muscles are relaxed, some air can escape and the abdominal wall can distend, leaving the skeletal framework to provide the required resistance to deformation.

Forces acting on the anterior chest wall are transmitted through the superficial tissue to the underlying bony skeleton. Internal stresses and strains are developed within the individual skeletal elements (e.g. ribs, sternum), which if sufficiently intense can cause fracture, joint dislocations, as well as pneumo-and/or hemothorax.

Chest injury tolerance and biomechanical behavior play an important role in the crashworthiness design of all transportation systems. This is particularly true for automobiles, since nonpenetrating injuries are the second leading cause of automobile crash fatalities, Kihlberg (1965). The concept of vehicle crashworthiness itself has as its objective occupant protection from injury. This end objective can only be sensibly achieved in concert with a thorough scientific understanding of the injury producing processes.

Scientists concerned with impact tolerance and biomechanical behavior of the human thorax have approached these problems from two directions; experimentally and analytically. Laboratory efforts typically focus upon experiments conducted upon human volunteers; Lobdell (1973), Patrick (1966), cadavers; Nahum (1975), Patrick (1975), Schmidt (1975), Kroell (1974, 1971), Lobdell (1973), Stalnaker (1973), and most recently Robbins (1976) and Eppinger (1978), animals; Schreck (1973), Shatsky (1974), or anthropometric dummies, Schmidt (1975). Analysts, on the other hand, have sought to create either lumped parameter models, which are in fact mathematical representations of laboratory data, Lobdell (1973), or basic structural dynamic representations of the actual thorax, Chen (1978, 1974), Roberts (1975, 1974, 1971), Reddi (1977), Andriacchi (1974)*. This second analytical approach offers the only possibility for ever gaining a fundamental conceptual understanding of injury processes and thereby a predictive capability applicable to a wide variety of circumstances. It goes without saying that this objective can only be achieved by the sincere efforts of the experimentalist and analyst working cooperatively toward the same goal.

The THORAX V Model

The THORAX V model is a finite element representation of an average sized seated male (Fig. 1a, 1b). The major structural and mass components of the thoracic skeleton are represented as:

Head - Lumped mass

Ribs - Curved-twisted beam elements

Vertebral Column - Straight beam elements

Costal Cartilage - Straight beam elements

The overall dimensions are approximately those of a 50th percentile male, bearing in mind that the THORAX V dimensions are skeletal.

	THORAX V	50th percentile male
Height	-	68 in.
Seated Height	31.5 in.	35.7 in.
Chest depth	7.9 in.	9.0 in.
Chest circumference	34.6 in.	37.7 in.
Chest breadth	11.0 in.	-
Total weight	152.5 lbs. (estimated)	164 lbs.

* For additional references in all categories see McElhaney (1976), King (1975)

The model is geometrically midsagittally symmetric and fully three-dimensional (1074 D.O.F.) capable of accepting arbitrary spatially and temporally varying forcing functions. All material properties are linear elastic and small deformation theory is invoked. The total mass is distributed to the nodal points using data from Liu (1975).

The analysis is conducted on SAPV, using modal decomposition and superposition. The first fifty modes and frequencies are generated and then used in the SAP RESTART mode to analyse forced responses. A separate program has been written to calculate nodal point accelerations and plot the results.

Comparison of THORAX V Predictions with Experiments

The experimental data used for this study is contained in Robbins (1976, 1978), Eppinger (1978). These consist of filtered (100 Hz) recordings from accelerometers mounted at 8 locations on the skeleton of each of the tested cadavers. These locations and the corresponding THORAX V nodal points are given in the table below and in Fig. 2a, 2b.

Accelerometer Location	D.O.F.	D.O.F. No.	THORAX V N.P.
Upper Sternum	P-A	1	17
Lower sternum	P-A	1	120,121
Left Upper Ribs, at midaxillary line	R-L	2	45,46
Left Lower Ribs, at midaxillary line	P-A	1	134,135
Right Upper Ribs, at midaxillary line	R-L	2	52,53
Right Lower Ribs, at midaxillary line	P-A	1	140,141
T-1	I-S	3	9
T-1	P-A	1	9
T-1	R-L	2	9
T-12	I-S	3	174
T-12	P-A	1	174
T-12	R-L	2	174

Of interest in this study, is the data corresponding to

Frontal Impacts: 14 fps and 20 fps

Side Impacts: 14 fps and 20 fps

The acceleration time histories of the impacting piston are not contained in these references but were obtained from NHTSA.

Since the impactor is "rigid", its force-time history while in contact with the chest, is obtained by multiplying its acceleration profile by its mass (weight of impactor, 51.5 lbs). What is not known, is the exact location of the impactor and how this forcing function distributes itself over the 6 in. diameter impact area. This will be influenced by the intrinsic geometry of the cadaver chest, its posture relative to the impactor and the inherent "stiffness distribution" of the chest wall. Since none of this information is available for each cadaver, we used our best judgement to assign the spatial load distribution for each test studied.

The phasing of the forcing function over the contact area is also important. Since the chest wall geometry does not initially conform to the flat impactor face, some points on the impacting surface are in contact while others are not in contact. Since this was not measured, we modified some forcing function amplitudes slightly .

Based upon the available data, the following test cases were selected for comparison with THORAX V predictions .

Case	Impact	Sex	Ht.(cm)	Wt.(kg)	AIS
76T053	Frontal, 14 fps	M	176.8	83.7	0
77T083	Frontal, 20 fps	- *	-	-	-
76T062	Side, 14 fps	-	-	-	-
77T077	Side, 20 fps	M	175.5	73.7	3

*Information not available

Each of these cases is discussed below in detail. Since no phasing information is available, the THORAX acceleration peaks were aligned with those of the experiments. Frontal impact cases were modeled as midsagittally symmetric.

Evaluation of the THORAX V results for each of the 4 cases presented below should be made with the understanding that information on each of the following effects was not available and consequently could not be incorporated in the THORAX V model.

a) The detailed anatomy of each cadaver tested

b) The spatial and temporal (especially phasing) impact load distribution to the skeletal structure

c) The causes for some of the wide scatter in the data

d) The pre-impact posture of the test specimen

Significant structural differences exist between the side and frontal impact configurations. The sternum, a rather rigid flat plate, serves to distribute frontal loads to the individual ribs in proportion to the apparent stiffnesses they present to the sternum. As a consequence, the frontal impact case is less sensitive to spatial load distribution.

During side loading, the impactor is in contact with individual ribs and only the musculature and superficial tissues are present to "spread" the load. The natural curvature of the midaxillary region further enhances the possibility of intense local rib contact. Therefore, at this stage of development, one should not expect THORAX V predictions for side impact to correspond with the data as well as the frontal impact cases.

For both frontal and side loading, a number of spatial load distributions were investigated. As expected, we found that some nodal point accelerations were more sensitive than others and that the sensitivity decreased for points well removed from the area of load application.

76T053, FRONTAL IMPACT, 14 fps

The impactor acceleration pulse is shown in Fig. 3 with the THORAX V forcing function for this case, superimposed. The calculated acceleration time histories are shown in Figs. 4 thru 13. All peak values compare quite well except for the left and right lower ribs, where the predictions are significantly above the experimental data. This is probably attributable to the choice of the spatial load distribution which may be overloading the lower ribs somewhat. This could be investigated by a more elaborate parametric study than we have had the opportunity to run.

Further insight can be gained by comparing the peak values given in Table 1. The R-L readings are omitted since THORAX V assumes the frontal impact to be midsagittally symmetric whereas the data shows some lack of symmetry which is to be expected. All the signs do correspond, suggesting that all the nodal points are predicted to be moving in the correct directions.

77T083, FRONTAL IMPACT, 20 fps

The forcing function used for this case is shown in Fig. 14. Since only four filtered accelerometer recordings were available, only four superimposed graphs are presented in Figs. 14 to 17. The peak values for the remaining data points were taken from the unfiltered curves and tabulated in Table 1.

TABLE 1

COMPARISON OF PEAK ACCELERATIONS (g's)

Location	D.O.F.	FRONT(14) 76T053 EXP.		FRONT(14) 76T053 THORAX V	FRONT(20) 77T083 EXP.		FRONT(20) 77T083 THORAX V	SIDE(14) 76T062 EXP.		SIDE(14) 76T062 THORAX V	SIDE(20) 77T077 EXP.		SIDE(20) 77T077 THORAX V
U.S.	P-A	-26	*	-32.4	-98	*	-94	9		8.4	2.5 -11		8.5 -11.8
L.S.	P-A	-78	*	-72.5	-153	*	-154	-10		-13.5	19 -21		19.7 -21.4
L.U.R.	R-L	7.5		7.4	17		23.9	-50	*	-20	-60	*	-33
L.L.R.	P-A	-12	*	-20.9	-29	*	-52	39		6.3	=		10.1
R.U.R.	R-L	-12		-5.9	-13		-23.4	-20	*	-15	-19.5	*	-23.9
R.L.R.	P-A	-7.5	*	-23.3	-25	*	-52	6.5		4.8	=		5.8
T-1	I-S	-5		-12.3	-28		-26.8	5.8		2.5	=		-1.3
T-1	P-A	-13	*	-20.3	-55	*	-51	-4		-3.6	=		-4.1
T-1	R-L	-		-	-		-	-17	*	-14.4	-19	*	-22.5
T-12	I-S	-4.6		-6.8	-31		-19	-3		-0.8	-10		-1.1
T-12	P-A	-2	*	-1.4	-48	*	-40.5	-2.7		-6	-20.5		-3.3
T-12	R-L	-		-	-		-	-26	*	-12	-12	*	-17.5

- Loading is midsagittally symmetric. These values should be zero.

= Test data unavailable

* Accelerometers oriented in same direction as loading

The predicted initial pulse shapes and upper sternum amplitude correspond fairly well with the experiments. At most other points THORAX V tends to overestimate the peak accelerations except at T-1 and T-12 where again the correspondence is quite good.

76T062, SIDE IMPACT, 14 fps

The forcing function shown in Fig. 18 is delivered to the left side in the lateral-medial direction. As previously mentioned, the response of the upper and lower left side accelerometers will be strongly dependent upon the exact contact condition. This is demonstrated by the poor correlation obtained for these points (Figs. 21, 22). However, at points distant from the contact area, the response tends to be more dependent upon the total load time history, than the spatial distribution. We observe better correlation at the sternum, right side ribs and some of the vertebral column degrees of freedom, (Figs. 19, 20, 23 to 28). Again the peak values are compared in Table 1.

77T077 SIDE IMPACT, 20 fps

The forcing function and results for this case are presented in Figs. 31 to 41. Many of the predicted peak amplitudes compare reasonably well with the data as can be seen from Table 1. In this case, as well as for 76T062 we observe that THORAX V tends to predict lower frequency response characteristics than is present in the data. This suggests that in side impact, the superficial tissue and musculature may play a more significant role in stiffening the chest wall and distributing the load than in frontal loading where the sternum serves this role.

Summary, Conclusions and Suggestions for Future Work

The THORAX V structural dynamic model of a 50th percentile male skeleton was exercised using loading functions from two frontal and two side impact experiments. A comparison of the predicted acceleration profiles to their corresponding experimental results can be made from the accompanying graphs and by a review of the peak values assembled in Table 1. For completeness, the calculated displacement time histories for each accelerometer station are also plotted (Appendix A) although no displacement data is available for comparison.

The purpose of this project was to examine the feasibility of using THORAX V as an analytic tool to support cadaver experiments and dummy design and evaluation. Considering the limitations necessarily imposed upon the THORAX V model, (these are discussed in the body of the report), the results obtained clearly support the conclusion that the use of THORAX V is feasible and that it can make an important contribution.

This is not to say that the model in its current form can be used as a black box for any and all experimental conditions. The results of the side loading cases combined with the wide scatter in some of the experimental data speaks to the contrary. Additional studies, especially of the side loading conditions are suggested. More detailed information about each specimen and the conditions peculiar to each test set-up should be monitored and incorporated in the analytic model.

We are encouraged by these results and believe that continued development and improvement of this existing capability is justified. To this end we offer the following suggestions for current applications and

and future development efforts closely allied with experimental programs at other centers.

Current Applications

(1) Parametric studies of the effects of spatial and temporal load distributions

(2) Study the effects of cadaver posture and skeletal anatomy

(3) Calculation of seat belt and chest belt loads from sled test simulations

(4) Fill out lost of missing data channels from experimental results

(5) Determine effects of higher modes upon response parameters

Some Thoughts on Future Developments

(1) Complete the development of techniques for determining skeletal geometry of each tested cadaver

(2) Conduct parametric studies of the effects of skeletal geometry upon response parameters and injury production

(3) Incorporate injury criteria within THORAX

(4) Study effect of tensing voluntary chest muscles upon skeletal injury

(5) Study of a closed glottis upon chest stiffening

(6) Study the chest-impactor contact problem

(7) Incorporate effect of involuntary muscles (e.g. inter-costals) upon internal forces within the skeleton elements

Acknowledgment

This work was sponsored in part by the Department of Transportation/ National Highway Traffic Safety Administration under P.O. NHTSA 9-6577. This material represents the position of the author and not necessarily that of the Department of Transportation/NHTSA.

References

1. Andriacchi, T. et al (1974), "A Model for Studies of Interactions between the Human Spine and Rib Cage," Journal of Biomechanics, Vol. 7, pp. 497-507.

2. Chen, P. (1978), "Finite Element Dynamic Structural Model of the Human Thorax and Chest Impact Response and Injury Studies," Aviation, Space and Environmental Medicine, Vol. 49, No. 1, pp. 143-419.

3. Chen, P.H. and Roberts, S.B. (1974), "Dynamic Response of the Human Thoracic Skeleton to Impact," UCLA Paper ENG-0274, 1974.

4. Eppinger, R.H. et al (1978), "Development of a Promising Universal Thoracic Trauma Prediction Methodology," 22nd Stapp Car Crash Conference, pp. 209-268, Society of Automotive Engineers, Warrendale, Pa.

5. Kihlberg, J.K. (1965), "The Driver and His Right Front Passenger in Automobile Accidents," CAL Report VJ-1823-R16, Cornell Aeronautical Laboratory, Buffalo, N.Y.

6. King, A.I. and Chou, C.C. (1975), "Mathematical Modelling, Simulation and Experimental Testing of Biomechanical System Crash Response," presented at AIAA 11th Annual Meeting, AIAA Paper No. 75-272, Washington, D.C.

7. Kroell, C.K. et al (1971), "Impact Tolerance and Response of the Human Thorax," Proceedings of the 15th Stapp Car Crash Conference, pp. 84-134.

8. Kroell, C. et al (1974), "Impact Tolerance of the Human Thorax II," 18th Stapp Car Crash Conference, pp. 383-457, Society of Automotive Engineers, Warrendale, Pa.

9. Liu, Y.K. and Wickstrom, J.K. (1975), Estimation of the Inertial Property Distribution of the Human Torso from Segmented Cadaveric Data.

10. Lobdell, T. et al (1973), "Impact Response of the Human Thorax," Human Impact Response (edited by W. King and H. Mertz), pp. 201-246, Plenum Press, New York.

11. McElhaney, J., Roberts, V., Hilyard, J. (1976), Biomechanics of Trauma, Duke University, Durham, N.C.

12. Naclerio, E. (1975), Chest Injuries, Physiologic Principles and Emergency Management, Grune and Strathm, New York.

13. Nahum, A. et al (1975), "Cadaver Skeletal Response to Blunt Thoracic Impact," 19th Stapp Car Crash Conference, pp. 259-294, Society of Automotive Engineers, Warrendale, Pa.

14. Patrick, L., et al (1966), "Impact Dynamics of Unrestrained, Lap-belted and Lap and Diagonal Chest Belted Vehicle Occupants," 10th Stapp Crash Conference, pp. 46-93, Society of Automotive Engineers, Warrendale, Pa.

15. Patrick, L. and Levine, R. (1975), "Injury to Unembalmed Belted Cadavers in Simulated Collisions," 19th Stapp Car Crash Conference, pp. 79-116, Society of Automotive Engineers, Warrendale, Pa.

16. Reddi, M.M. and Tsai, H.C. (1977), "Computer Simulations of Human Thoracic Skeletal Response," Vol. 1 and 2, Final Report, DOT HS 803209, U.S. Dept. of Transportation, NHTSA.

17. Robbins, D.H. (1978) "Quantification of Thoracic Response and Injury," Report on Contract DOT HS-4-00921, February 1978.

18. Robbins, D.H., et al (1976), "The Prediction of Thoracic Impact Injuries," Proceedings 20th Stapp Car Crash Conference, Society of Automotive Engineers, Warrendale, Pa.

19. Roberts, S.B. and Chen, P.H. (1971), "On Some Geometric Properties of Human Ribs - I," Symposium on Biodynamic Models and Their Applications, publ. by Aerospace Med. Res. Lab., WPAFB, Ohio (AMRL-TR-71-29), pp. 403-427.

20. Roberts, S.B. (1974), "The Dynamic Response of a Child's Thorax to Blunt Trauma," Proceedings of International Meeting on Biomechanics of Trauma in Children, pp. 237-245.

21. Roberts, S.B. (1975), "Intrusion of the Sternum with the Thoracic Cavity during Frontal Chest Impact and Injury Potential," Aircraft Crashworthiness, (edited K. Saczalski et al), pp. 253-272, University Press of Virginia, Charlottesville.

22. Schmidt, G. et al (1975), "Neck and Thorax Tolerance Levels of Belt-Protected Occupants in Head-On Collisions," 19th Stapp Car Crash Conference, pp. 225-258, Society of Automotive Engineers, Warrendale, Pa.

23. Schreck, R.M. and Viano, D.C. (1973), "Thoracic Impact: New Experimental Approaches Leading to Model Synthesis," Proceedings of 17th Stapp Car Crash Conference, Oklahoma City, Oklahoma, Society of Automotive Engineers, pp. 437-450.

24. Shatsky, S. (1974), "Traumatic Distortions of the Primate Head and Chest: Correlation of Biomechanical, Radiologic and Pathologic Data," 18th Stapp Car Crash Conference, pp. 351-381.

25. Stalnaker, R. et al (1973), "Human Torso Response to Blunt Trauma," Human Impact Response, (edited by W. King and H. Mertz) pp. 181-200, Plenum Press, New York.

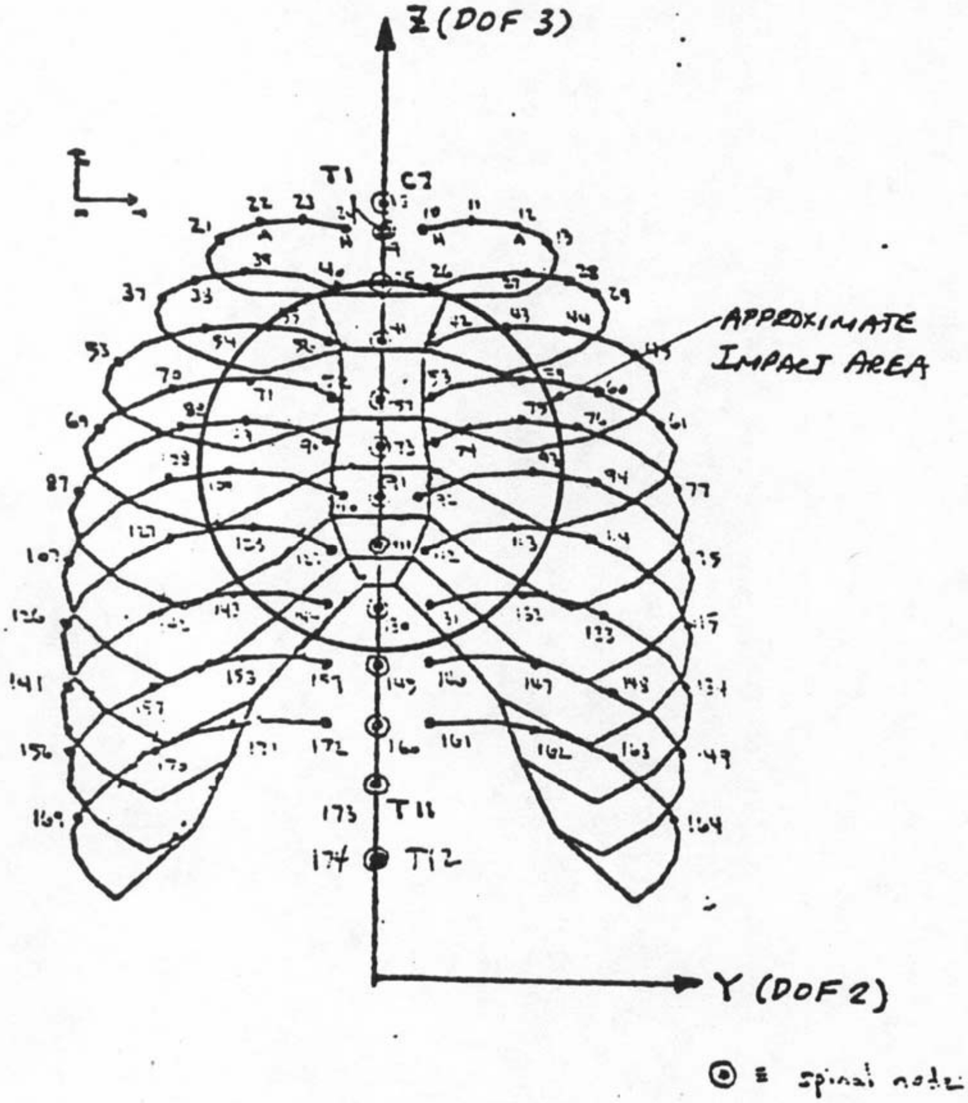

Fig. 1a_ THORAX V

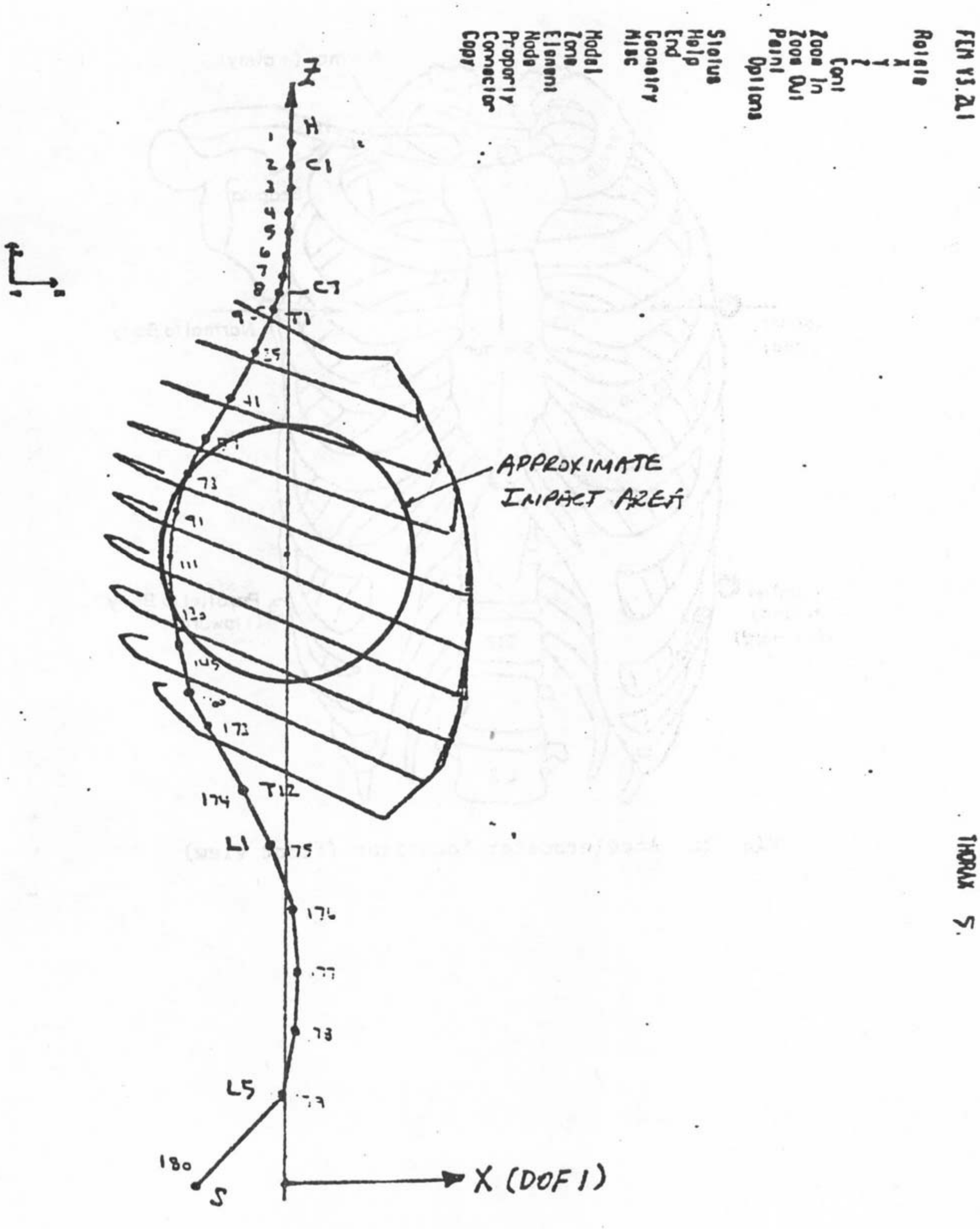

Fig. 1b THORAX V

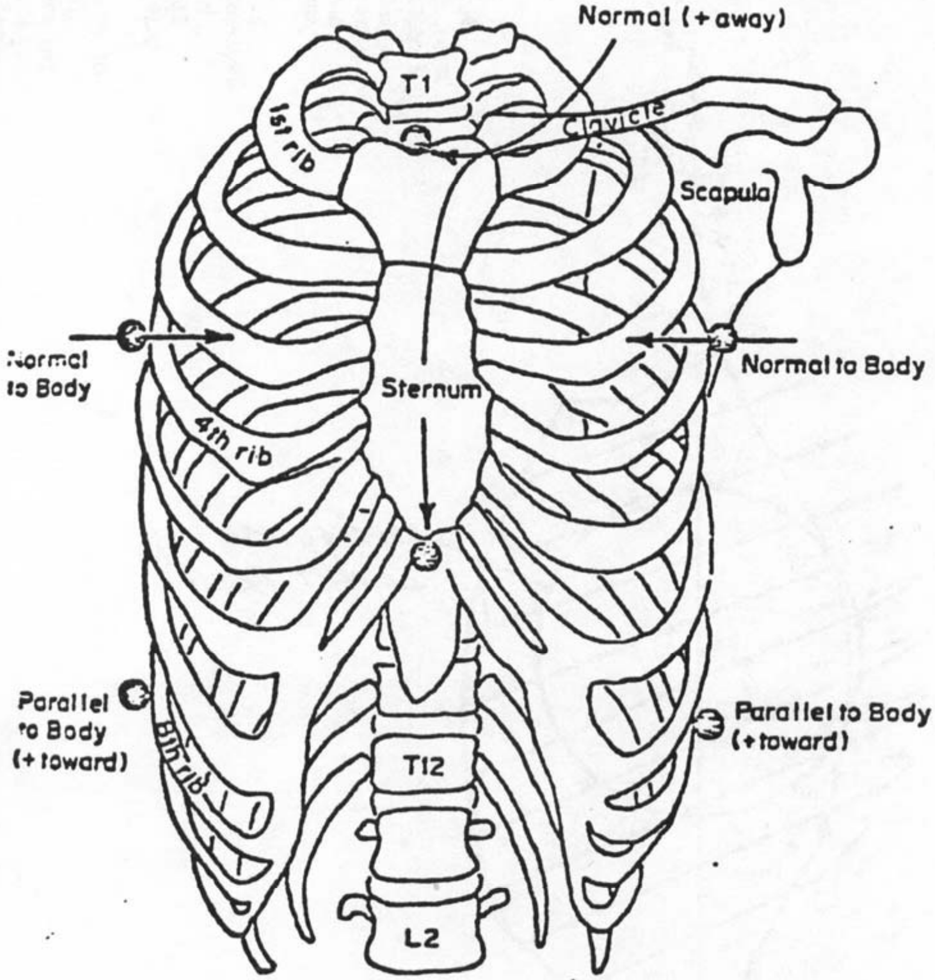

Fig. 2a Accelerometer locations (front view)

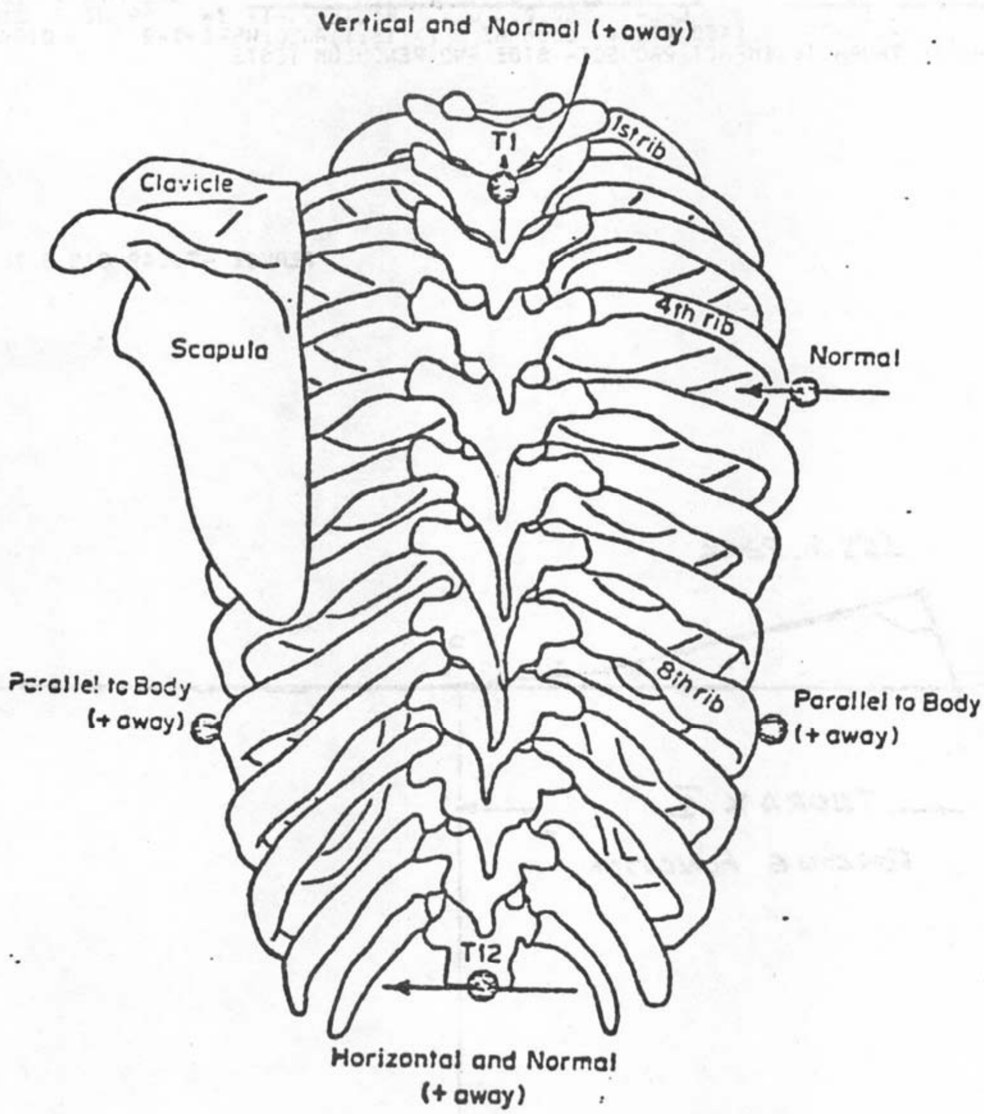

Fig. 2b Accelerometer locations (back view)

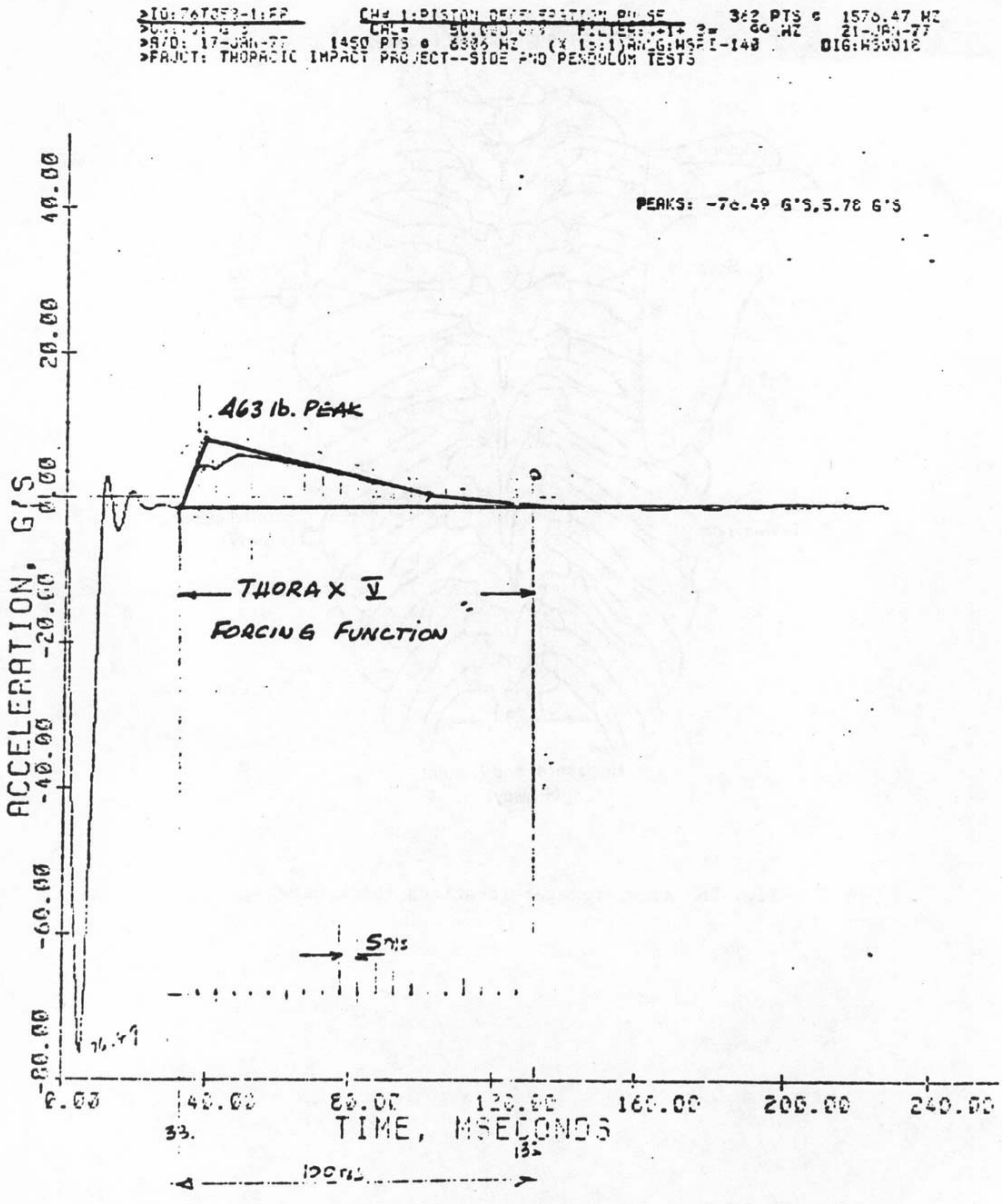
CH# 1:PISTON DECELERATION PULSE
362 PTS @ 1576.47 HZ
>R/D: 17-JAN-77
1450 PTS @
21-JAN-77
>PRJCT: THORACIC IMPACT PROJECT--SIDE AND PENDULUM TESTS
PEAKS: -76.49 G'S,5.78 G'S
463 lb. PEAK
THORAX V
FORCING FUNCTION
5ms
76.49
ACCELERATION, G'S
40.00
20.00
0.00
-20.00
-40.00
-60.00
-80.00
0.00
40.00
80.00
120.00
160.00
200.00
240.00
TIME, MSECONDS
33.
133
100ms

Fig. 3

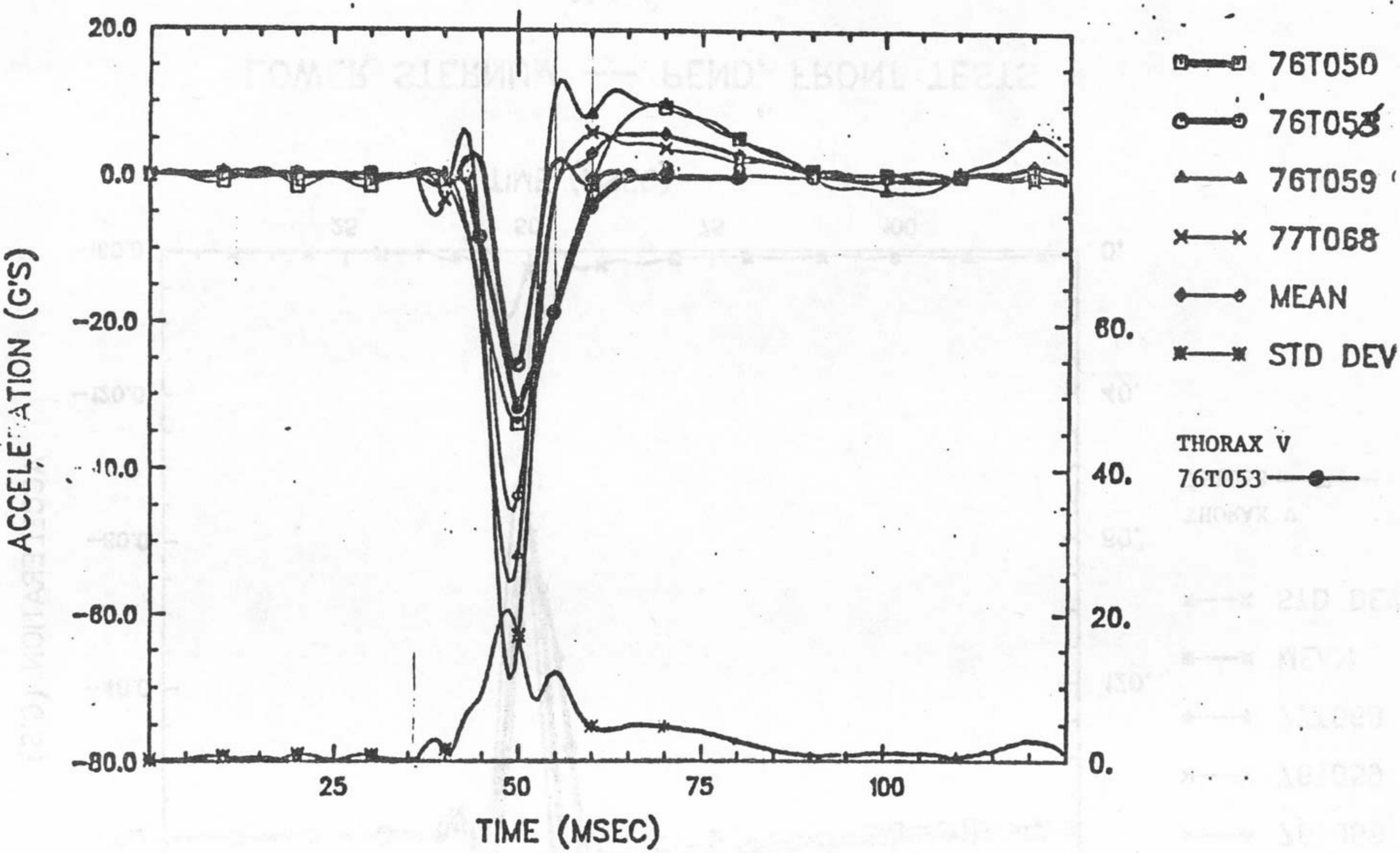

UPPER STERNUM -- PEND. FRONT TESTS

Fig. 4

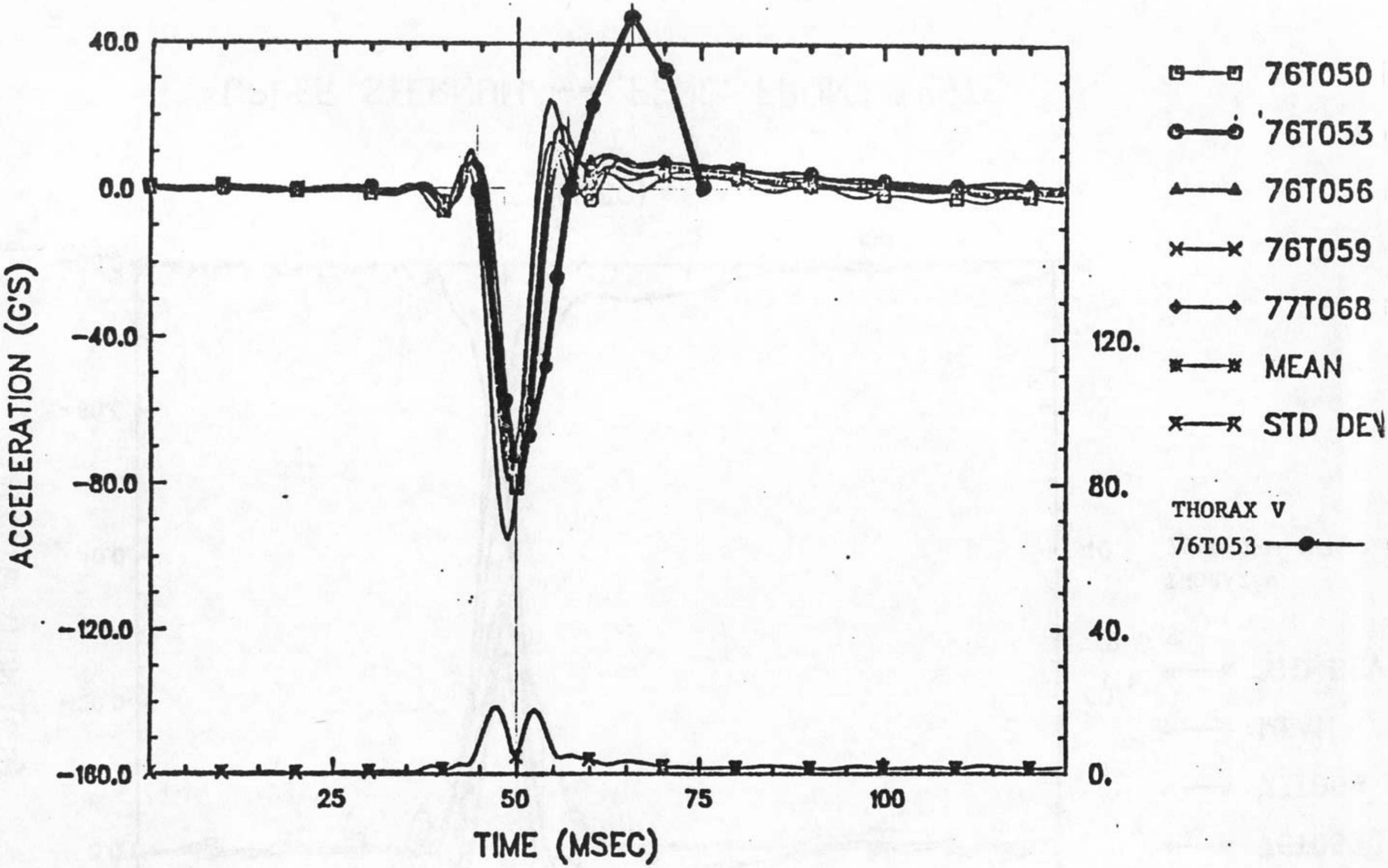

LOWER STERNUM -- PEND. FRONT TESTS

Fig. 5

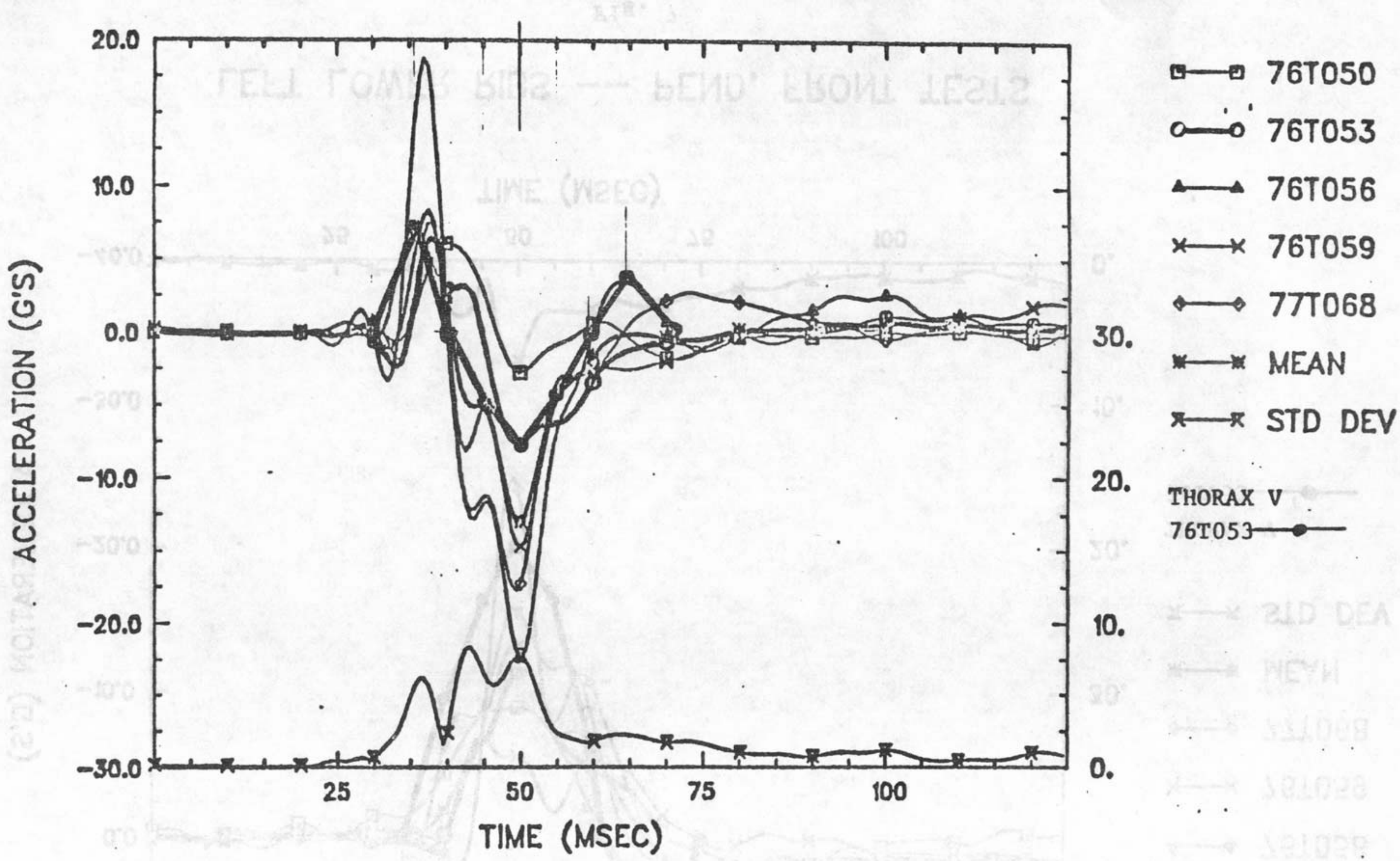

LEFT UPPER RIBS -- PEND. FRONT TESTS

Fig. 6

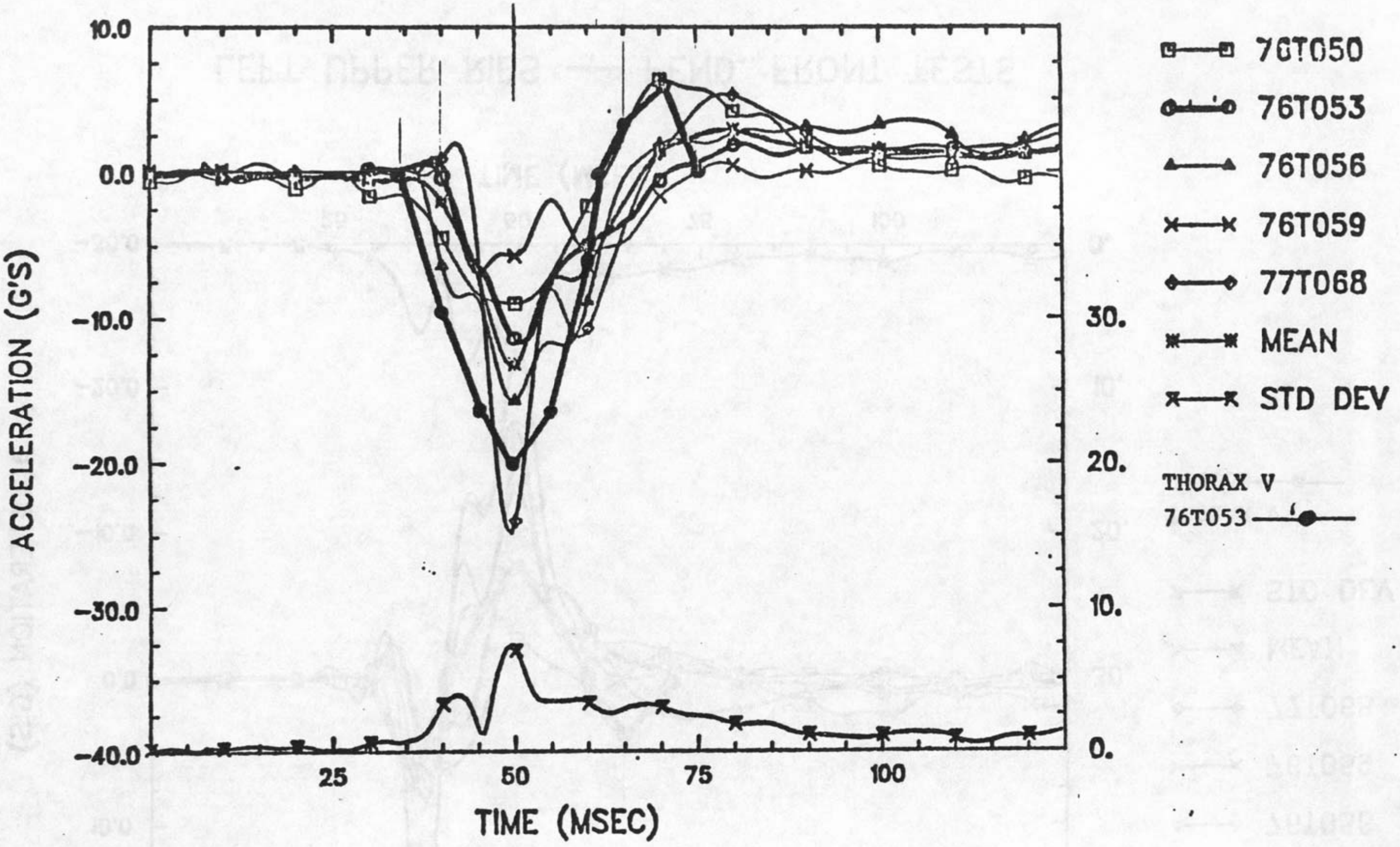

LEFT LOWER RIBS -- PEND. FRONT TESTS

Fig. 7

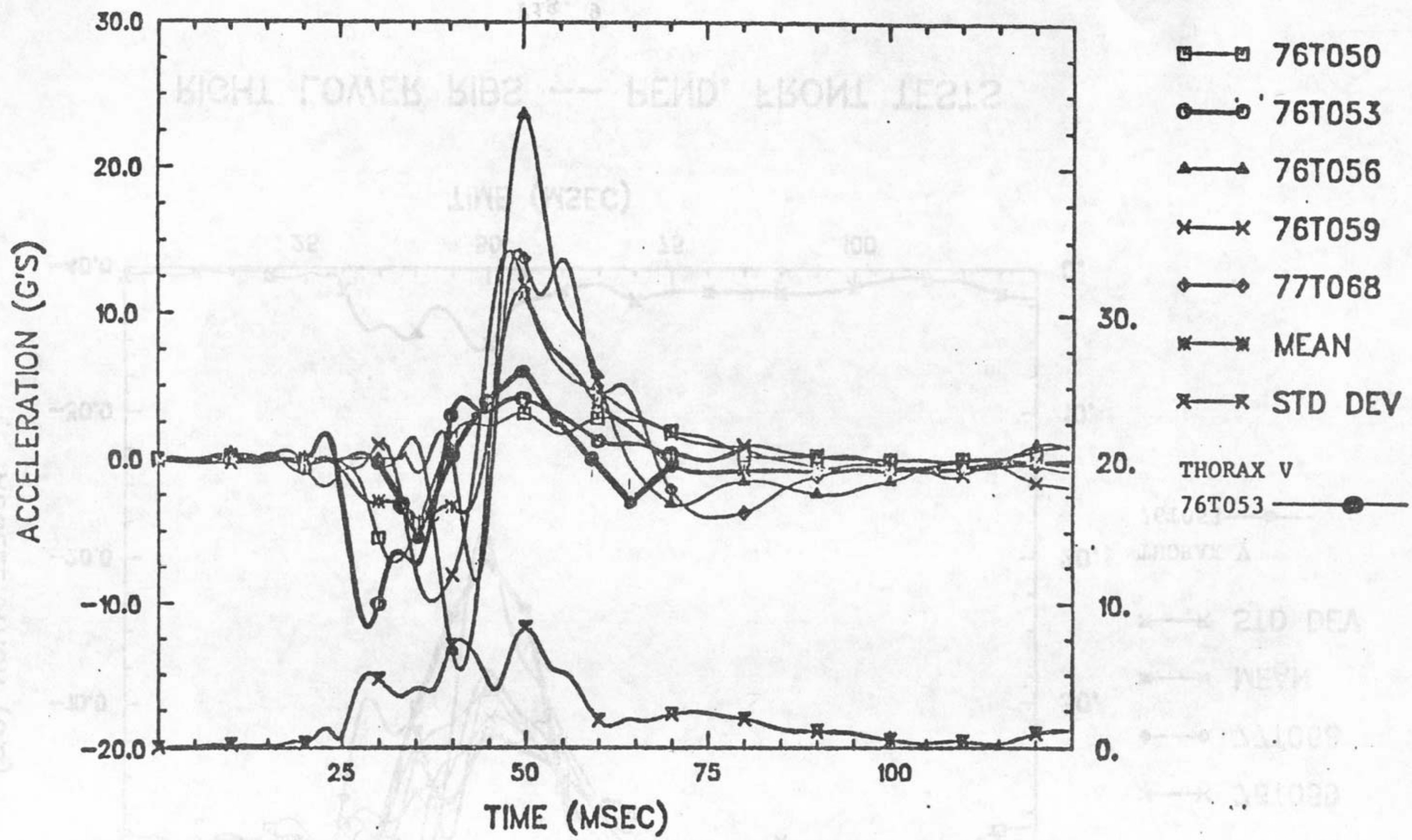

RIGHT UPPER RIBS — PEND. FRONT TESTS

Fig. 8

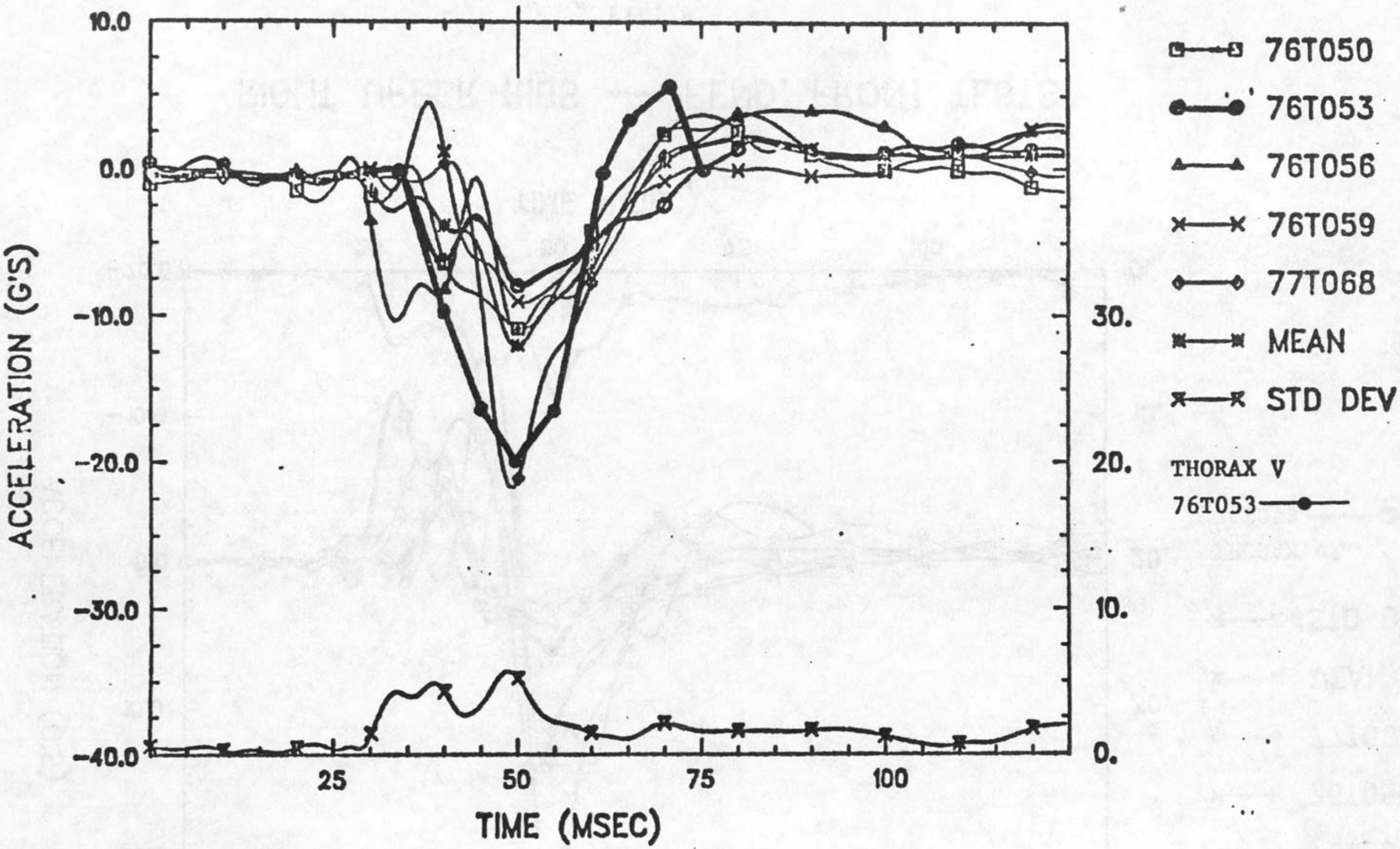

RIGHT LOWER RIBS --- PEND. FRONT TESTS

Fig. 9

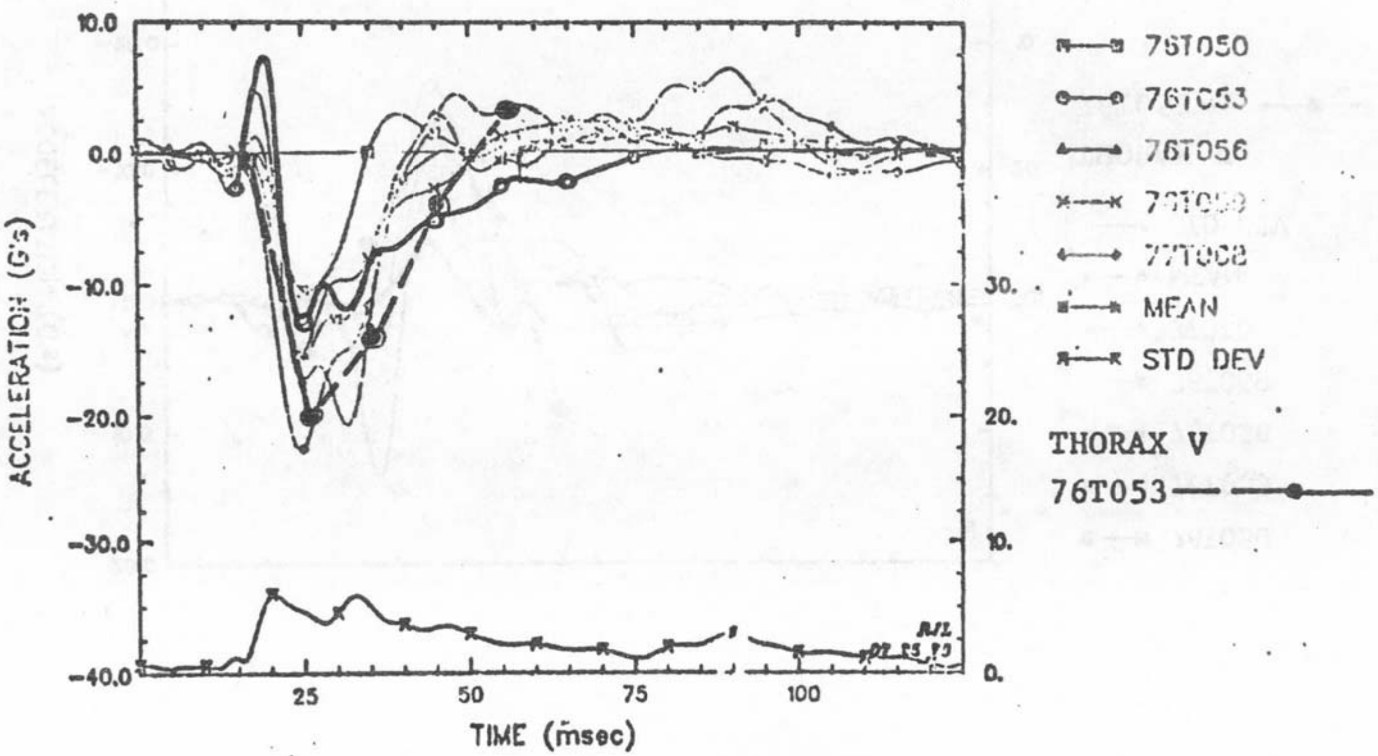

- T1 P-A accelerometer - pend. front test

Fig. 10

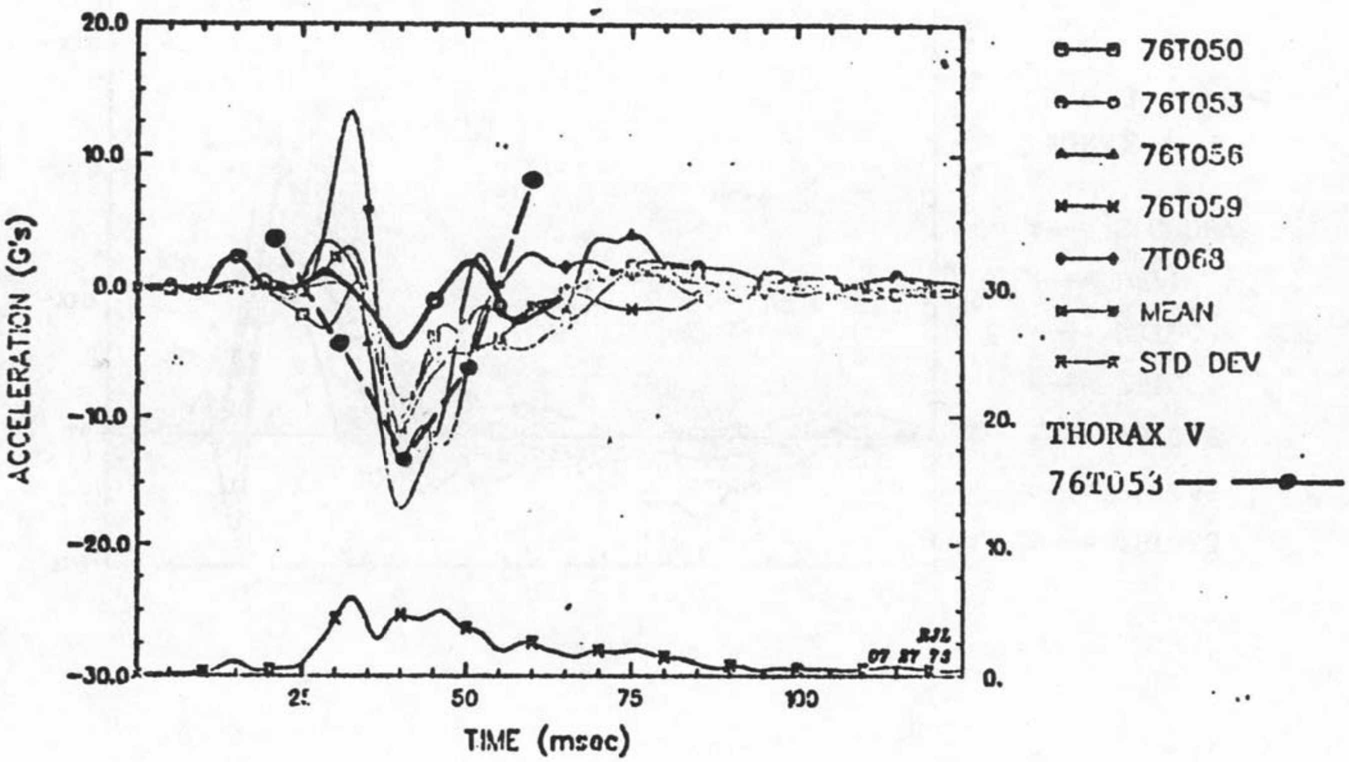

• T1 I-S accelerometer - pend. front test

Fig. 11

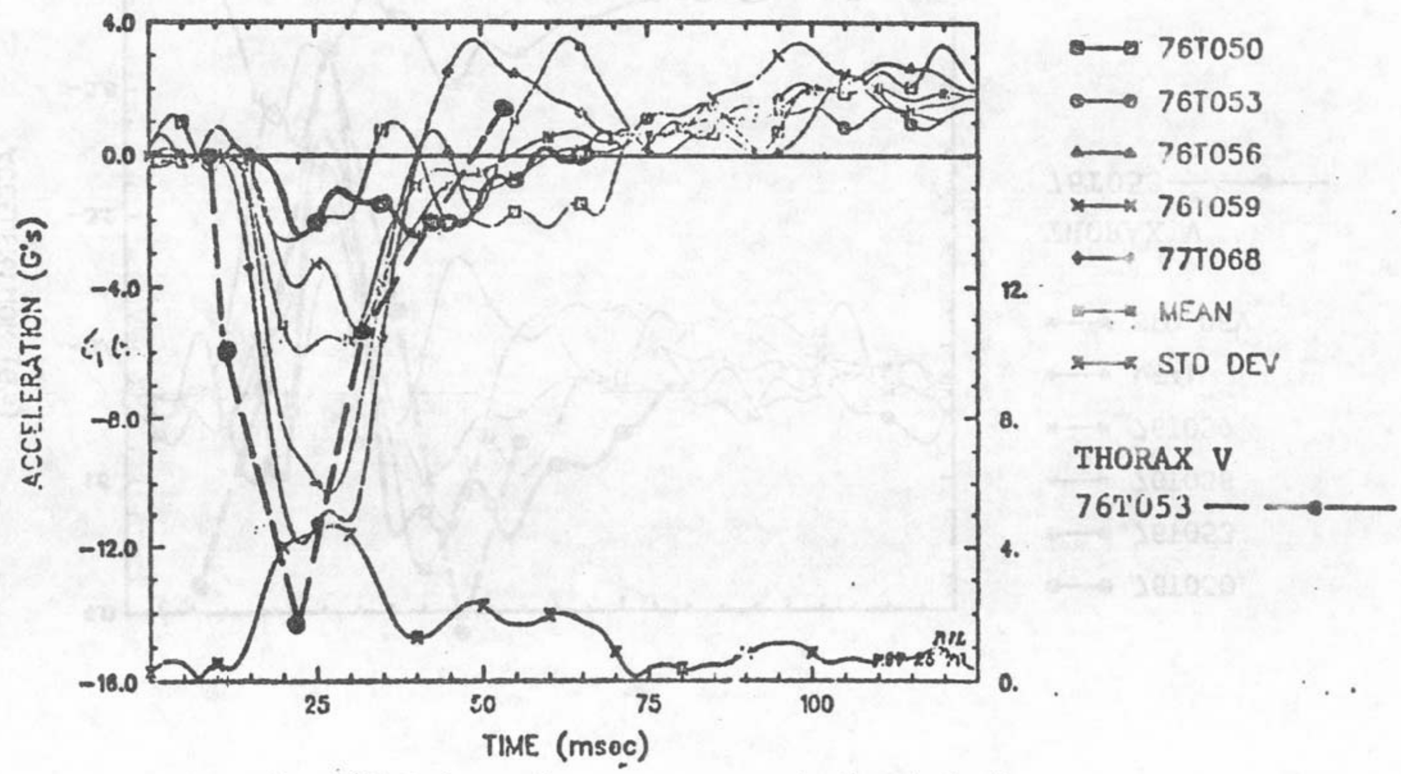

- T12 P-A accelerometer - pend. front test

Fig. 12

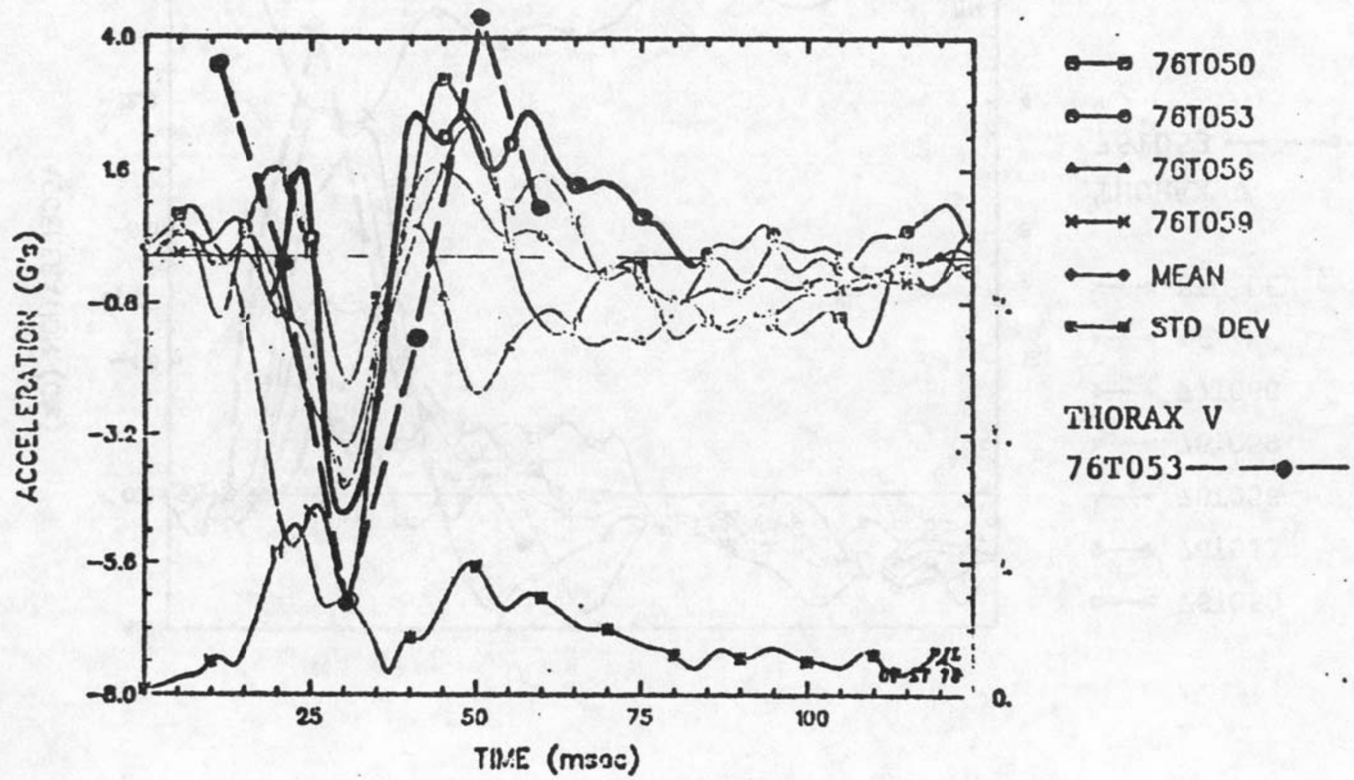

T12 I-S accelerometer - pend. front test

Fig. 13

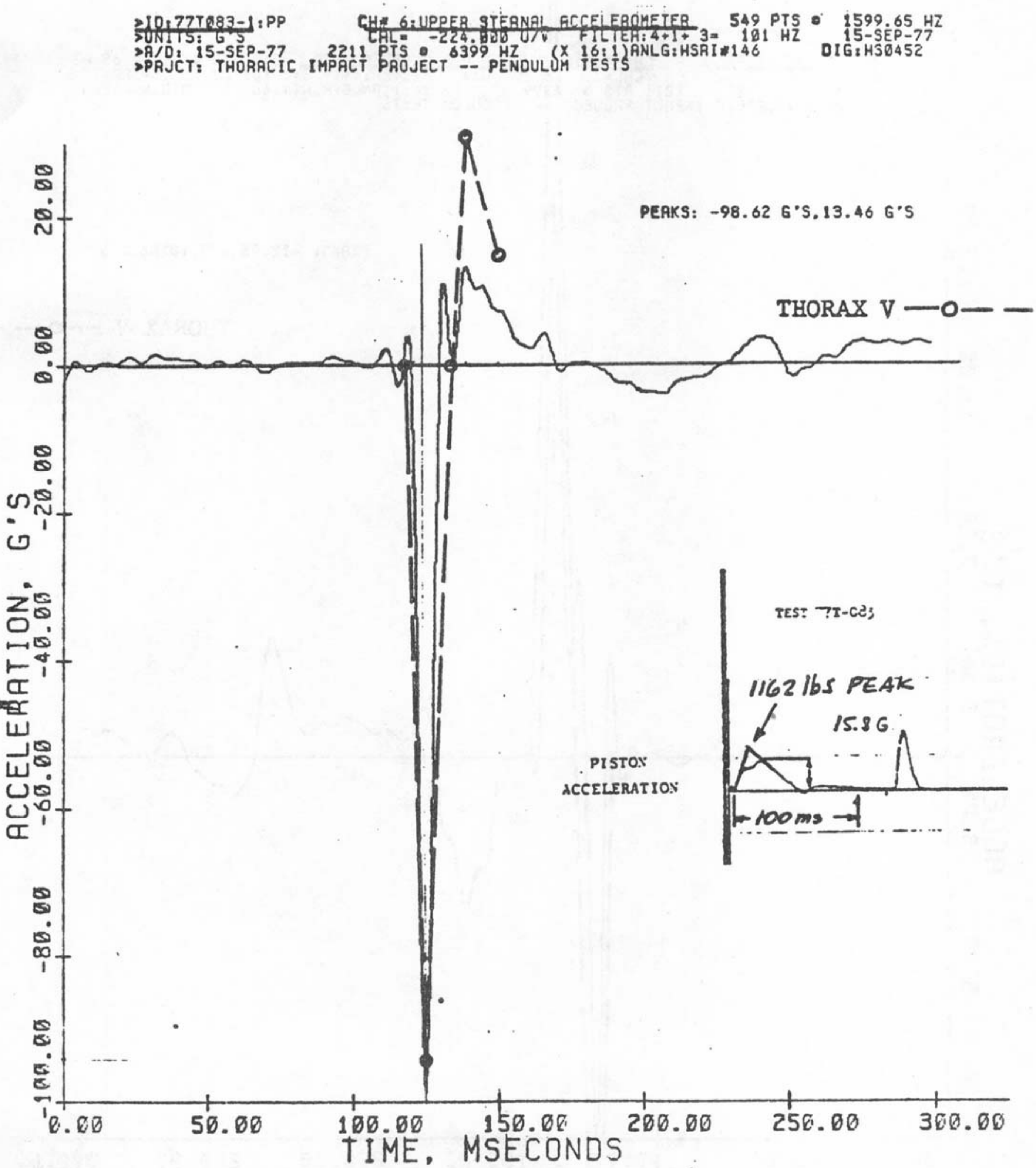
>ID:77T083-1:PP CH# 6:UPPER STERNAL ACCELEROMETER 549 PTS @ 1599.65 HZ
>UNITS: G'S CAL= -224.800 U/V FILTER:4+1+ 3= 101 HZ 15-SEP-77
>A/D: 15-SEP-77 2211 PTS @ 6399 HZ (X 16:1)ANLG:HSRI#146 DIG:H30452
>PRJCT: THORACIC IMPACT PROJECT -- PENDULUM TESTS
PEAKS: -98.62 G'S,13.46 G'S
THORAX V
TEST 77-C83
1162 lbs PEAK
15.8 G
PISTON ACCELERATION
100 ms
ACCELERATION, G'S
20.00
0.00
-20.00
-40.00
-60.00
-80.00
-100.00
0.00
50.00
100.00
150.00
200.00
250.00
300.00
TIME, MSECONDS

Fig. 14

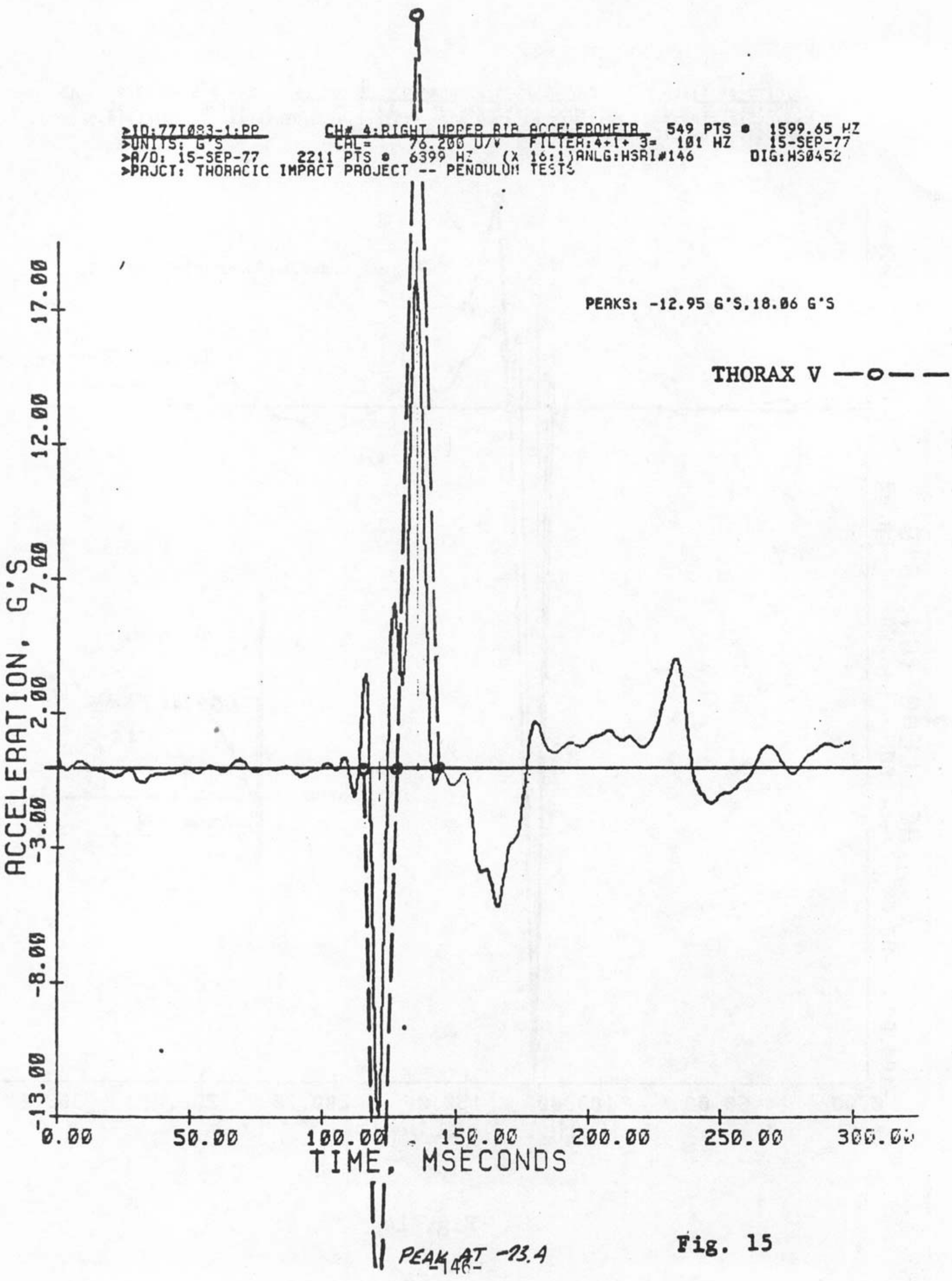

>ID:77T083-1:PP CH# 4:RIGHT UPPER RIB ACCELEROMETR 549 PTS @ 1599.65 HZ
>UNITS: G'S CAL= 76.200 U/V FILTER:4+1+ 3= 101 HZ 15-SEP-77
>A/D: 15-SEP-77 2211 PTS @ 6399 HZ (X 16:1)ANLG:HSRI#146 DIG:HS0452
>PRJCT: THORACIC IMPACT PROJECT -- PENDULUM TESTS
PEAKS: -12.95 G'S,18.06 G'S
THORAX V
ACCELERATION, G'S
17.00
12.00
7.00
2.00
-3.00
-8.00
-13.00
0.00
50.00
100.00
150.00
200.00
250.00
300.00
TIME, MSECONDS
PEAK AT -23.4

Fig. 15

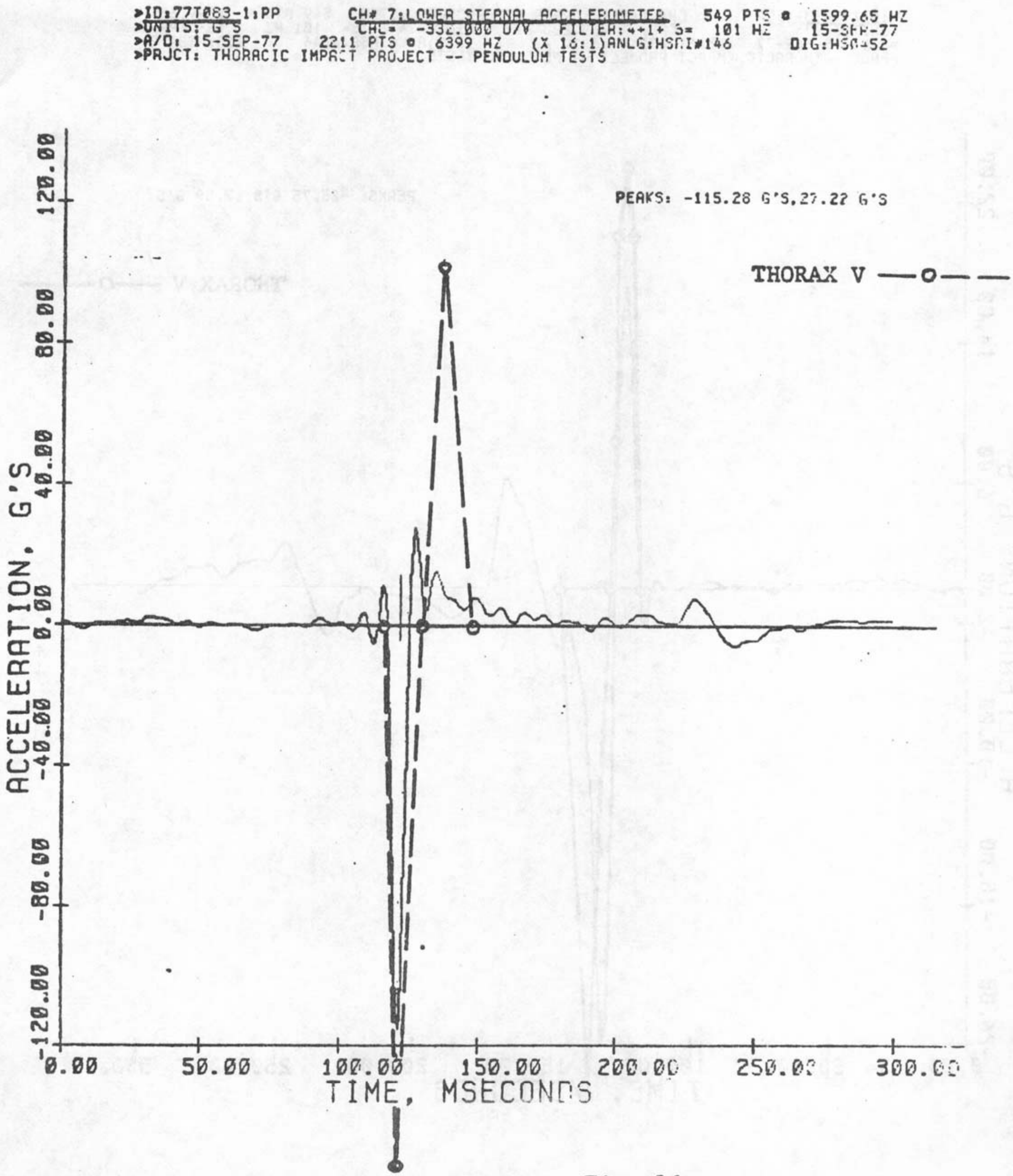
>ID:77T083-1:PP CH# 7:LOWER STERNAL ACCELEROMETER 549 PTS @ 1599.65 HZ
>UNITS: G'S CAL= -332.000 U/V FILTER:4+1+ 3= 101 HZ 15-SEP-77
>A/D: 15-SEP-77 2211 PTS @ 6399 HZ (X 16:1)ANLG:HSRI#146 DIG:HSR-52
>PRJCT: THORACIC IMPACT PROJECT -- PENDULUM TESTS
PEAKS: -115.28 G'S,27.22 G'S
THORAX V
ACCELERATION, G'S
120.00
80.00
40.00
0.00
-40.00
-80.00
-120.00
0.00
50.00
100.00
150.00
200.00
250.00
300.00
TIME, MSECONDS

Fig. 16

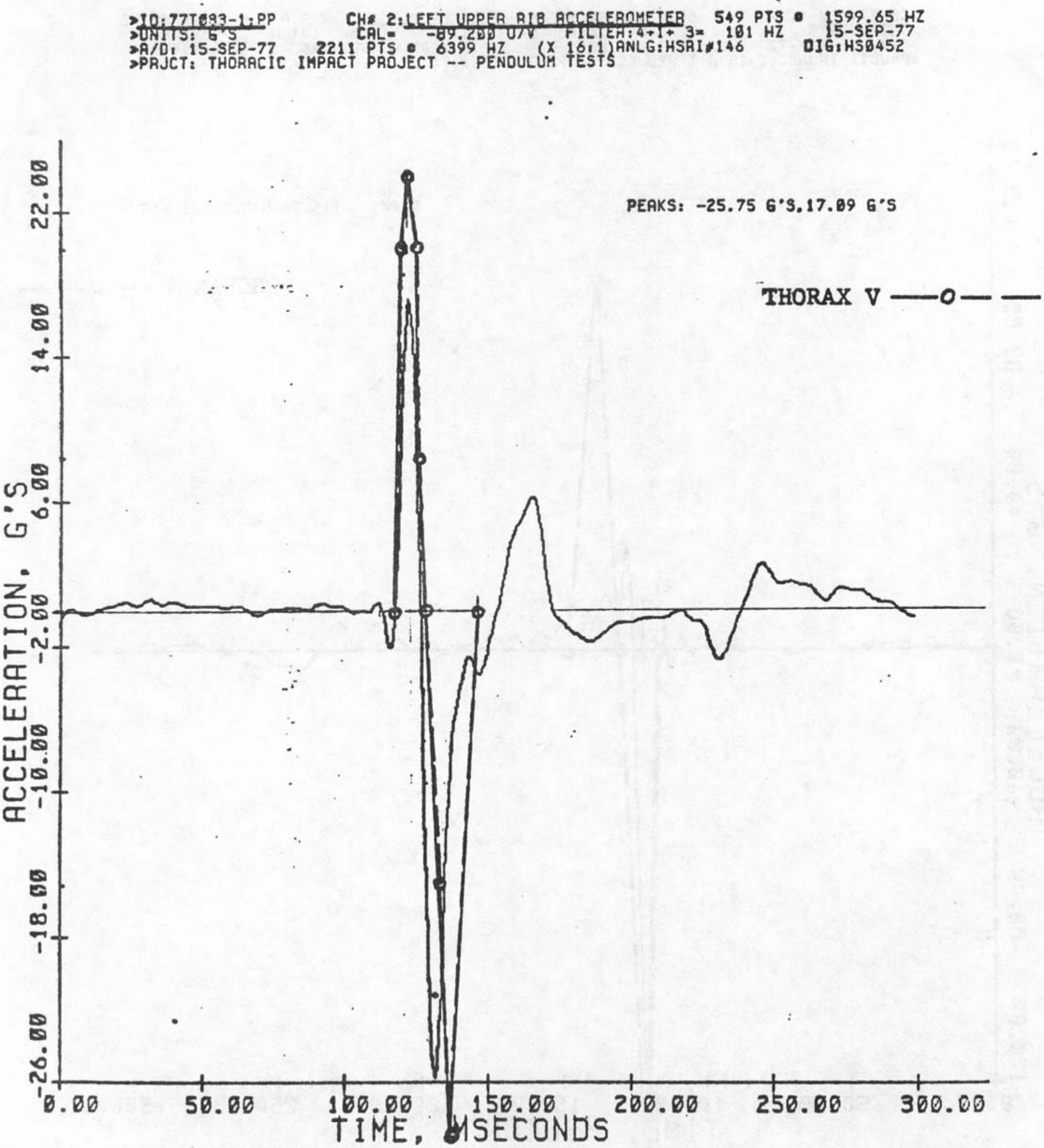
>ID:77T083-1;PP CH# 2:LEFT UPPER RIB ACCELEROMETER 549 PTS @ 1599.65 HZ
>UNITS: G'S CAL= -89.200 U/V FILTER:4+1+ 3= 101 HZ 15-SEP-77
>A/D: 15-SEP-77 2211 PTS @ 6399 HZ (X 16:1)ANLG:HSRI#146 DIG:HS0452
>PRJCT: THORACIC IMPACT PROJECT -- PENDULUM TESTS
PEAKS: -25.75 G'S,17.09 G'S
THORAX V
ACCELERATION, G'S
TIME, MSECONDS

Fig. 17

76T062
SIDE
14 FPS

>ID:76T062-1:PP CH# 1:PISTON DECELERATION PULSE 362 PTS @ 1576.85 HZ
>UNITS: G'S CAL= 30.000 U/V FILTER:4+1+ 3= 99 HZ 21-JAN-77
>A/D: 17-JAN-77 1447 PTS @ 6307 HZ (X 16:1)ANLG:HSRI-146 DIG:H30018
>PRJCT: THORACIC IMPACT PROJECT--PENDULUM TESTS

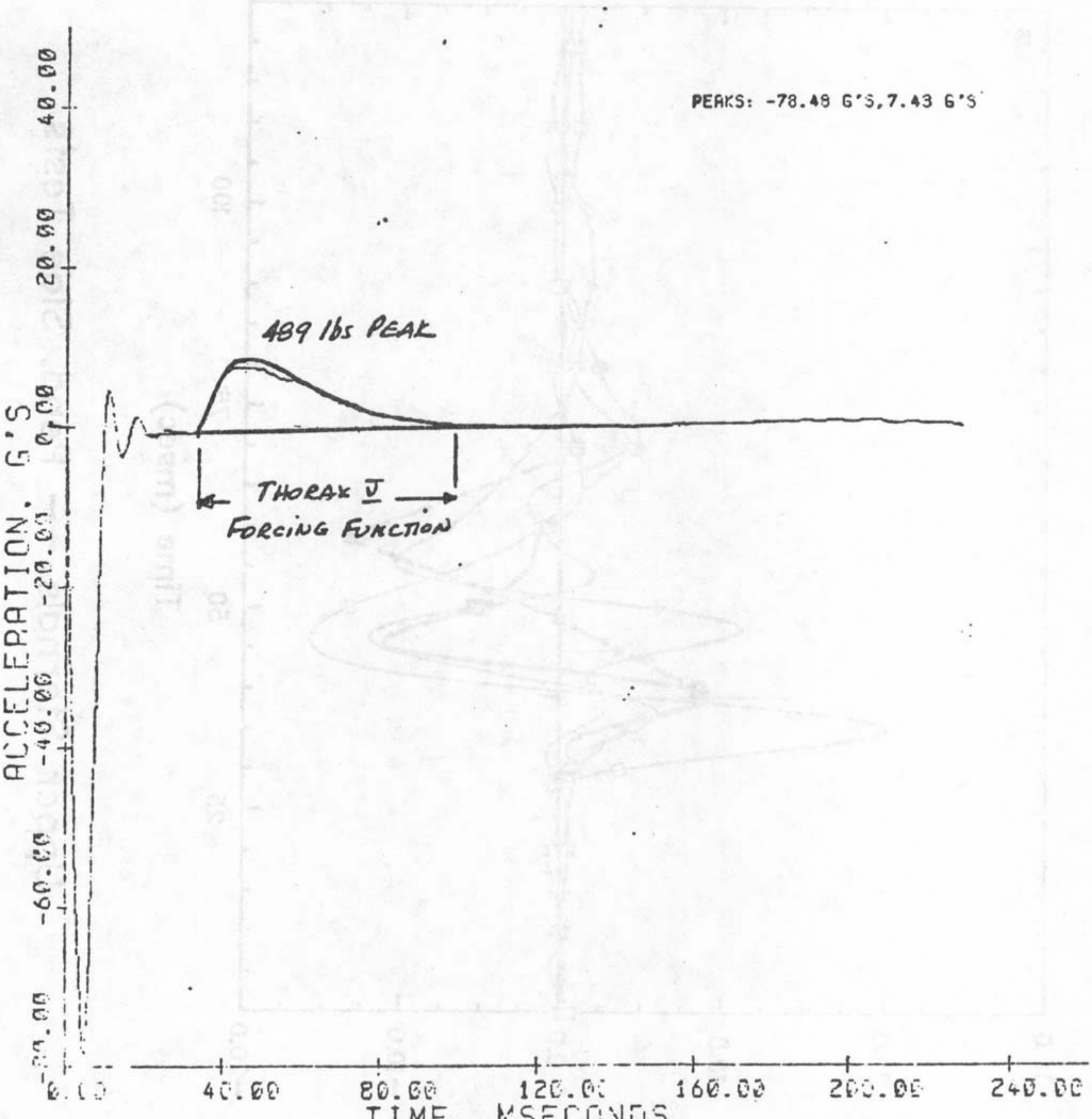

Fig. 18

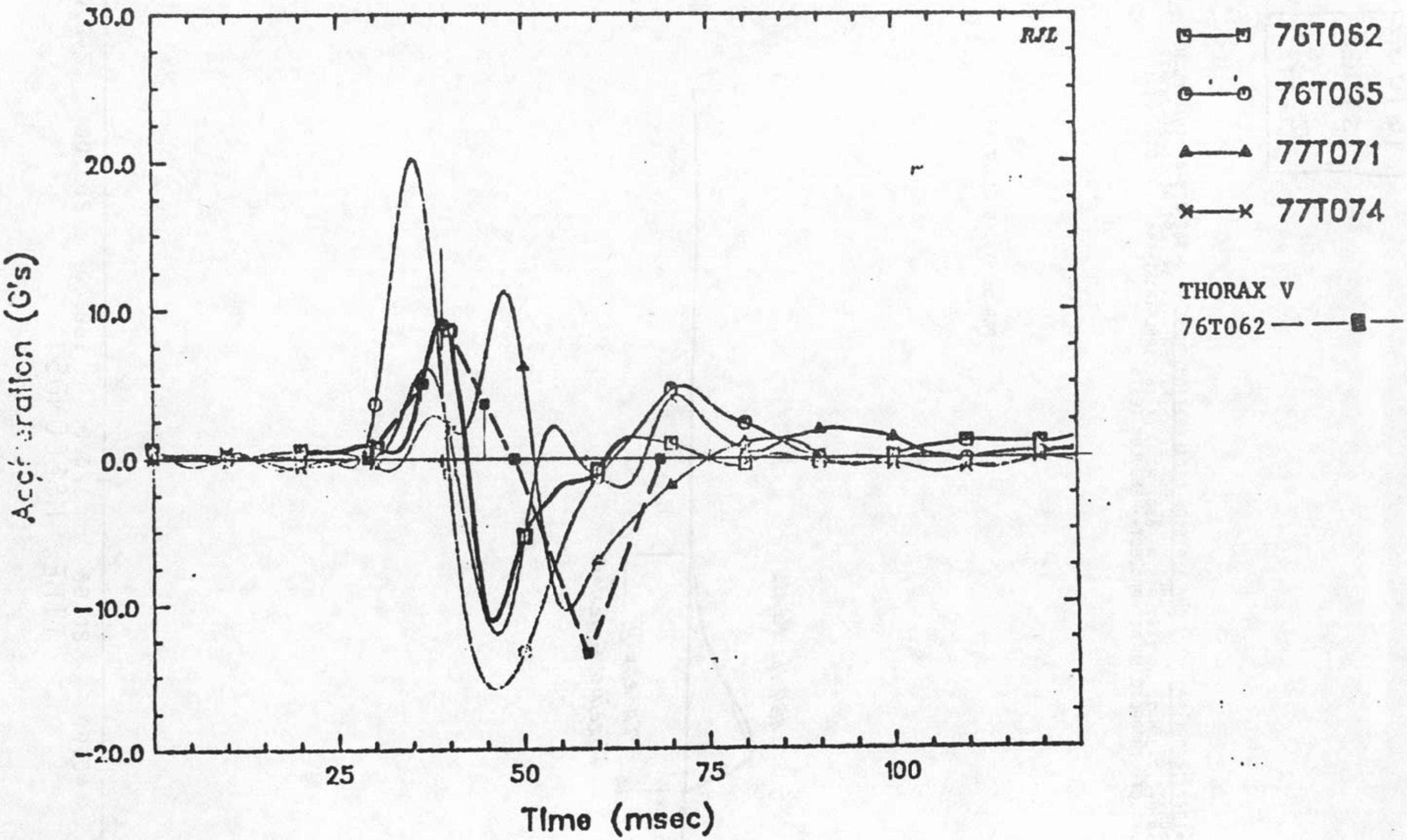

Upper Sternals -- Pend. Side Tests

Fig. 19

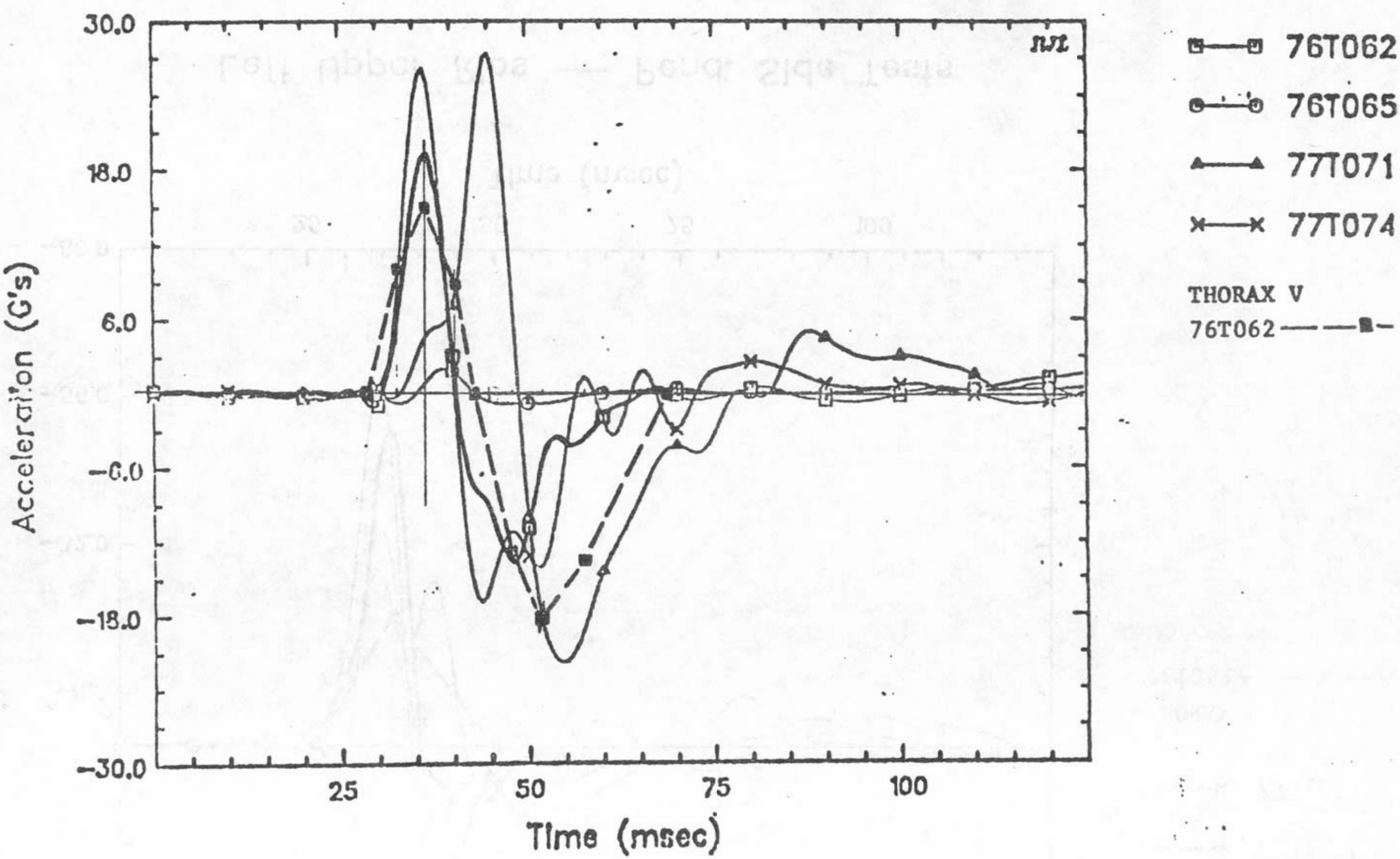

Lower Sternals -- Pend. Side Tests

Fig. 20

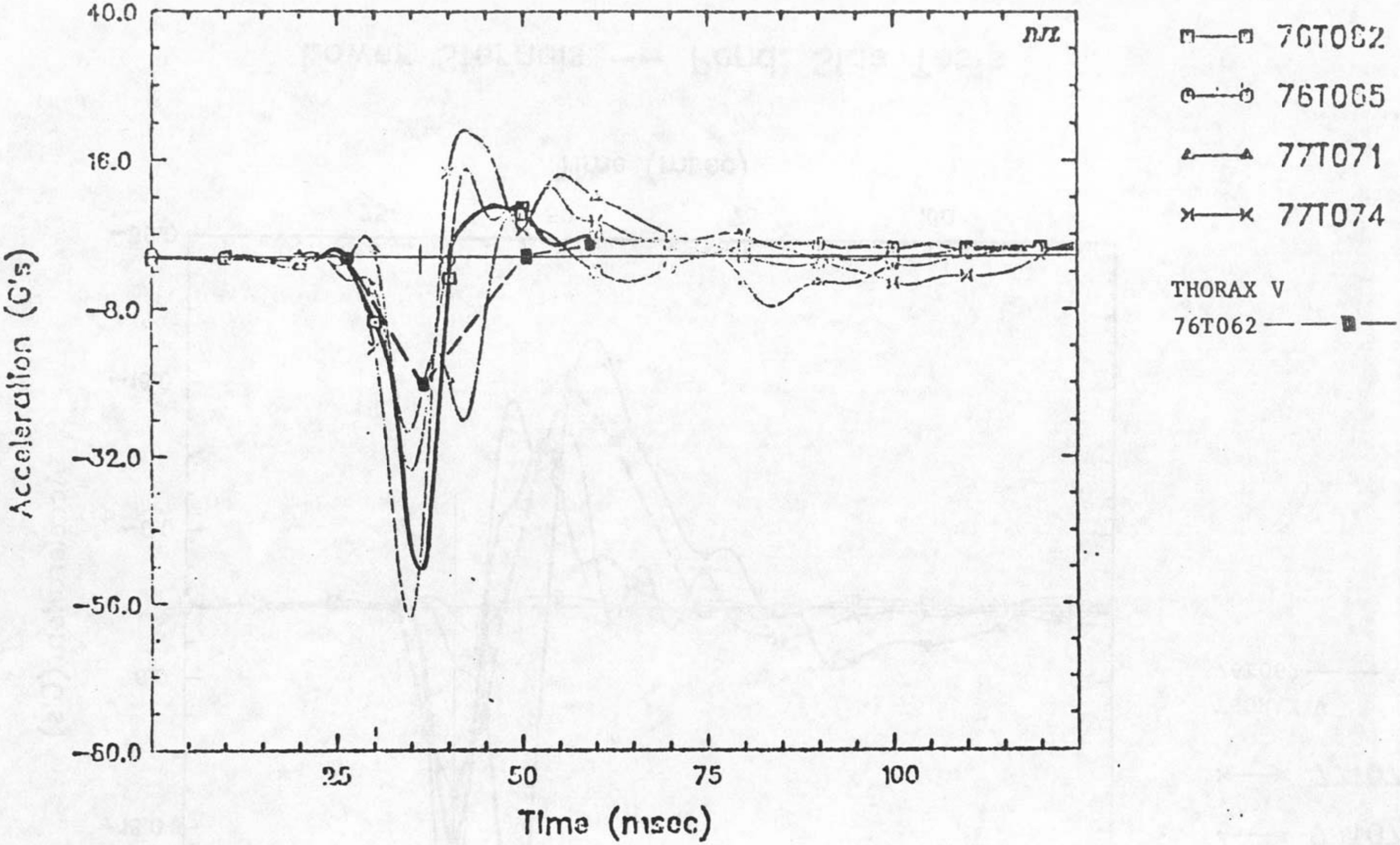

Left Upper Ribs --- Pend. Side Tests

Fig. 21

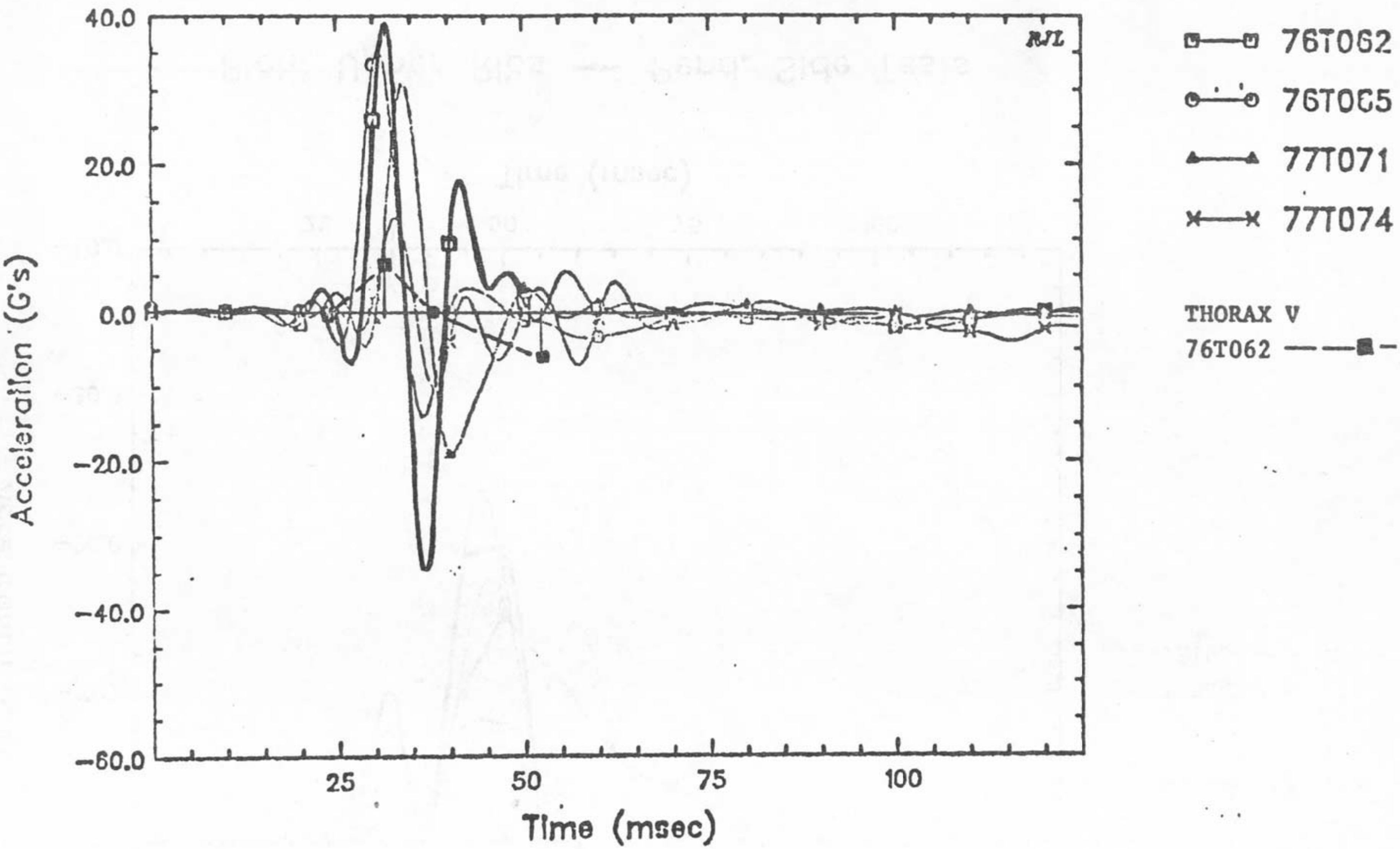

Left Lower Ribs -- Pend. Side Tests

Fig. 22

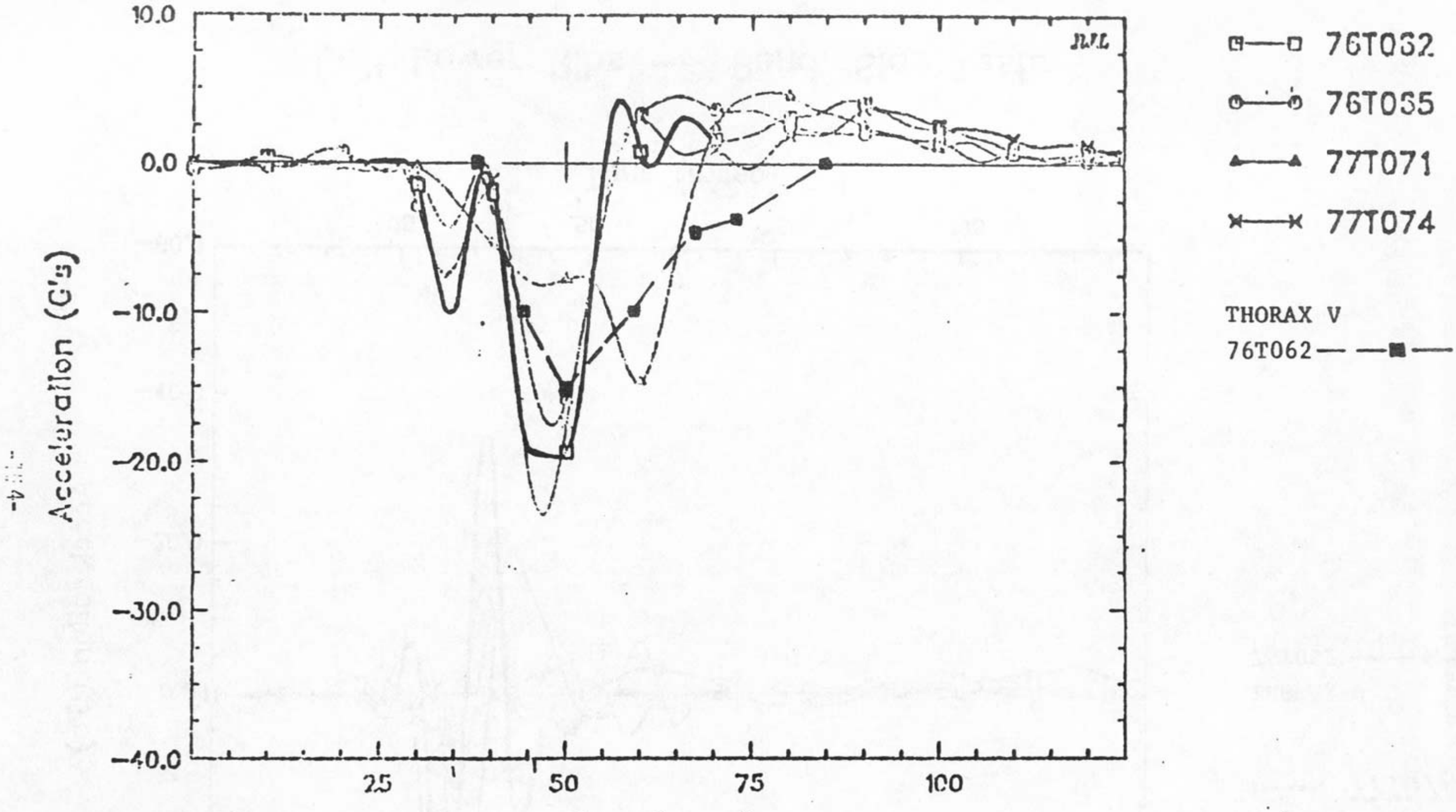

Right Upper Ribs -- Pend. Side Tests

Fig. 23

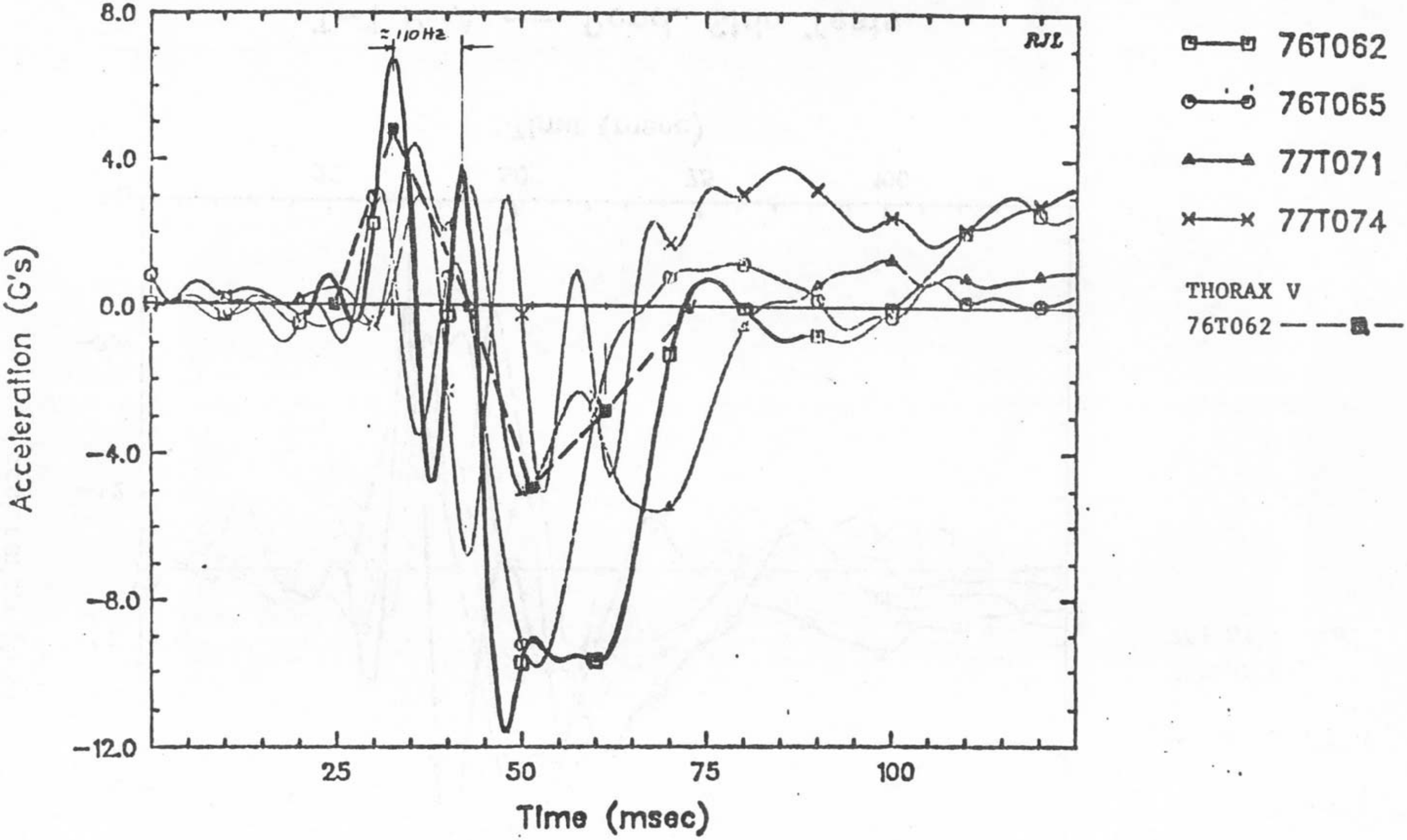

Right Lower Ribs —— Pend. Side Tests

/ Fig. 24/

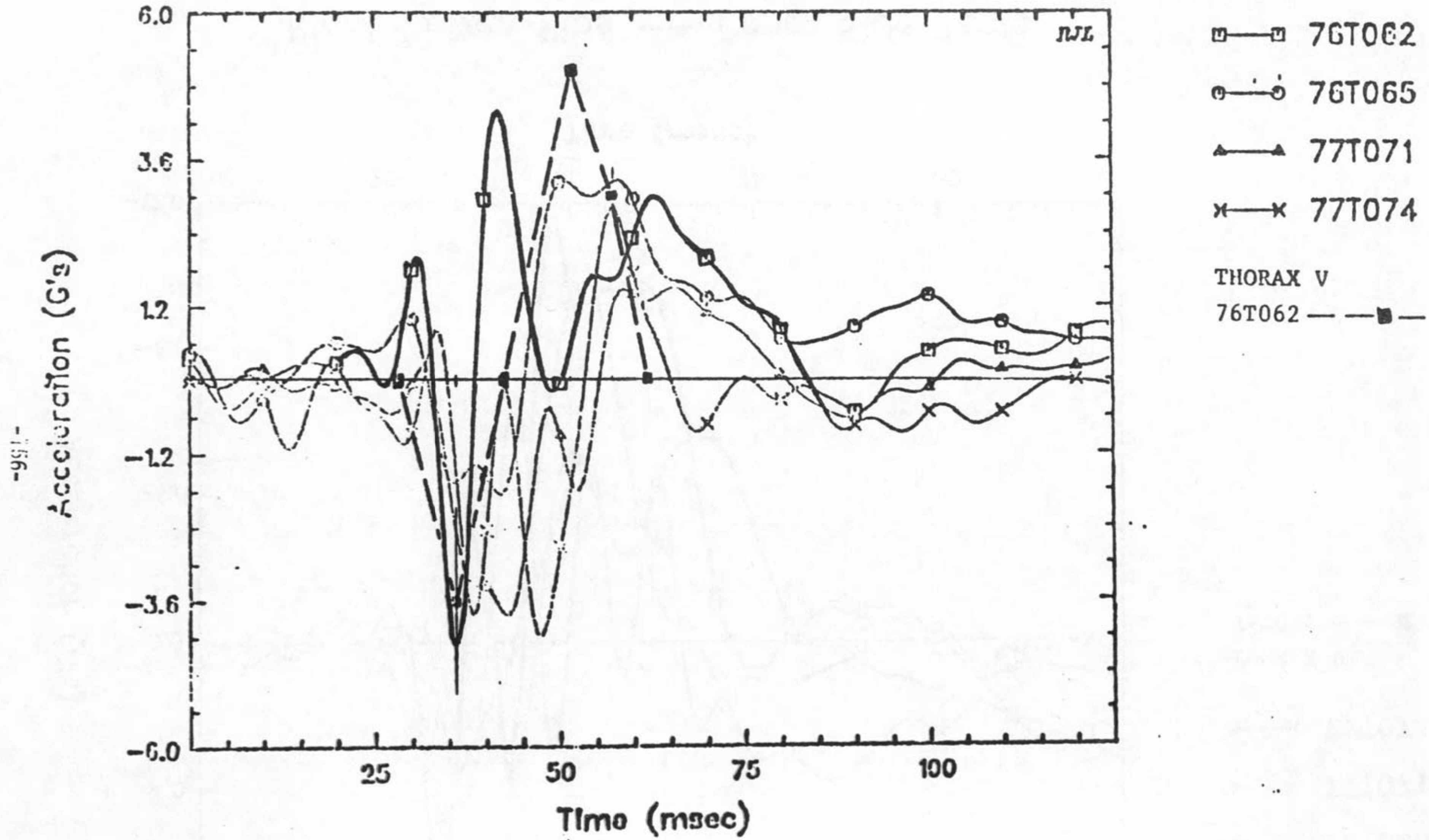

T-1 P-A —- Pend. Side Tests

Fig. 25

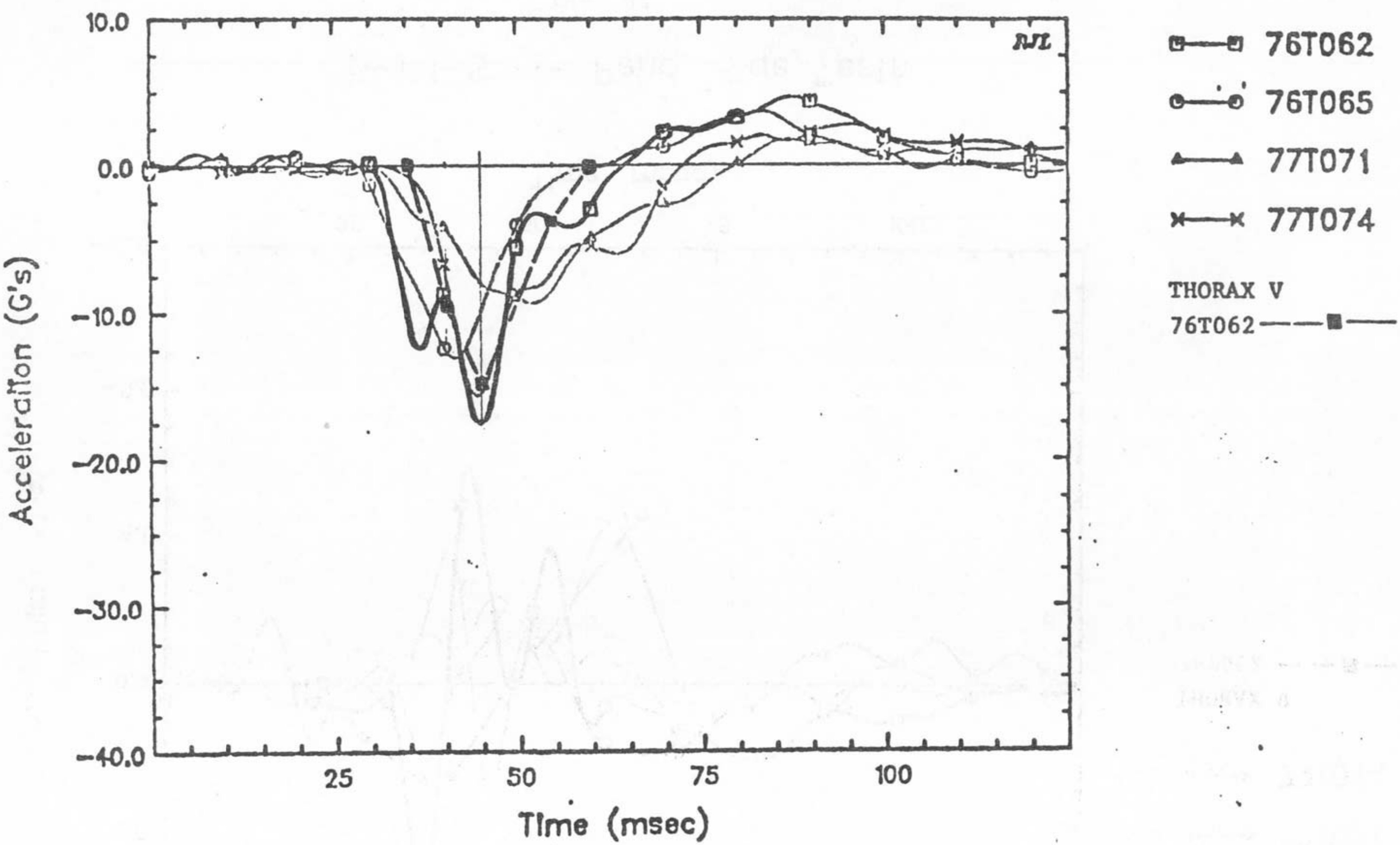

T-1 R-L --- Pend. Side Tests

Fig. 26

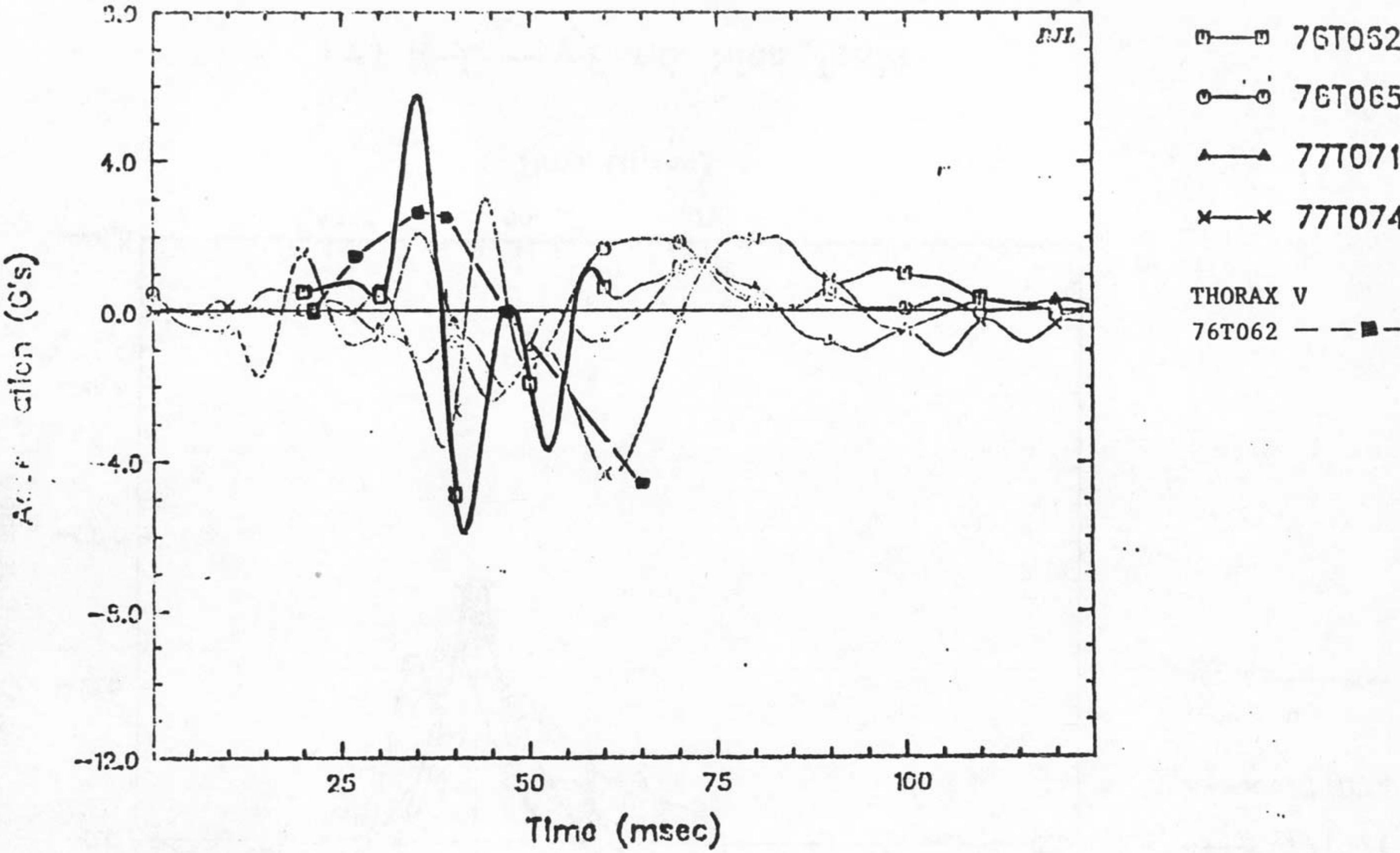

T-1 I-S — Pend. Side Tests

Fig. 27

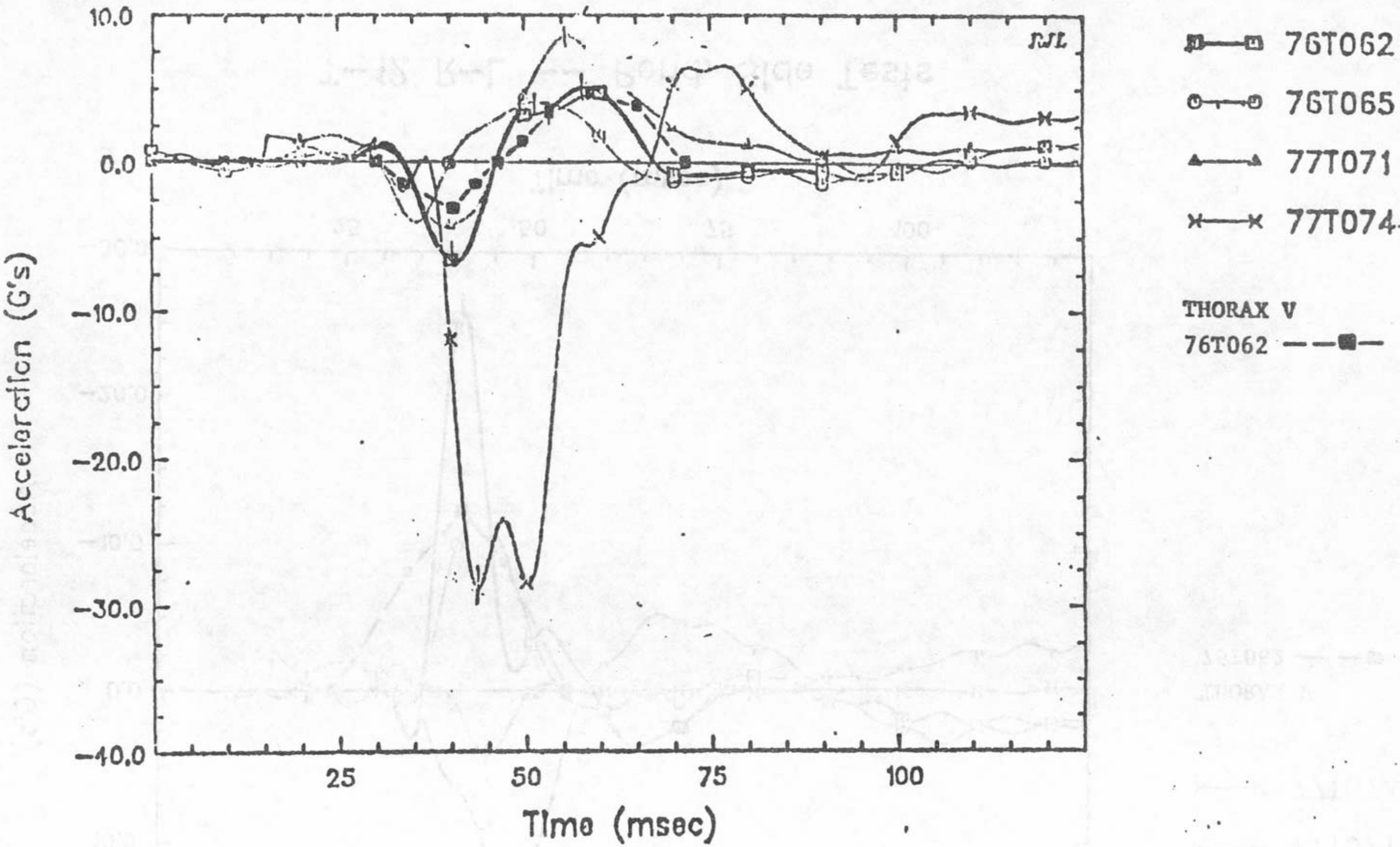

T-12 P-A --- Pend. Side Tests

Fig. 28

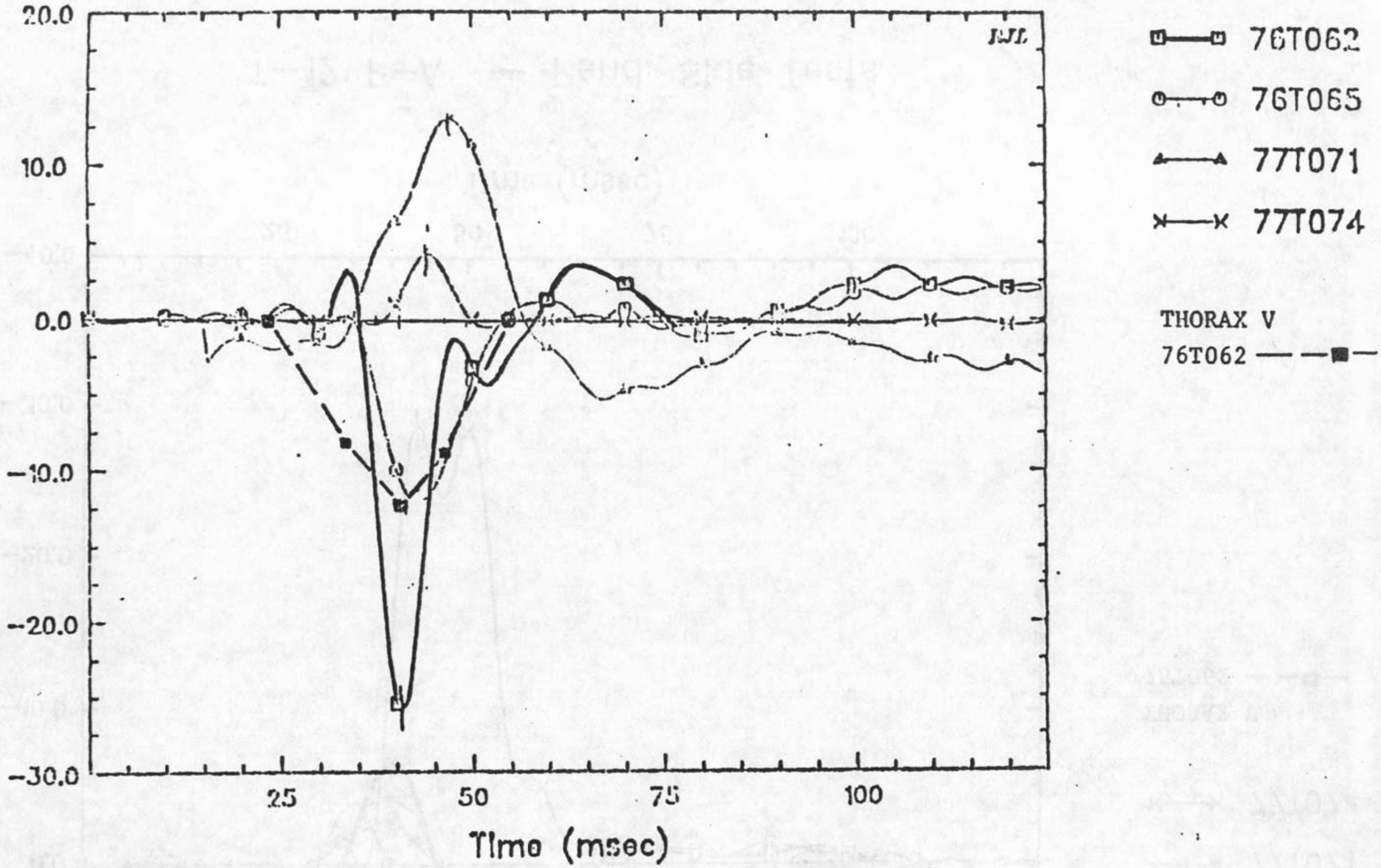

T-12 R-L -- Pend. Side Tests

Fig. 29

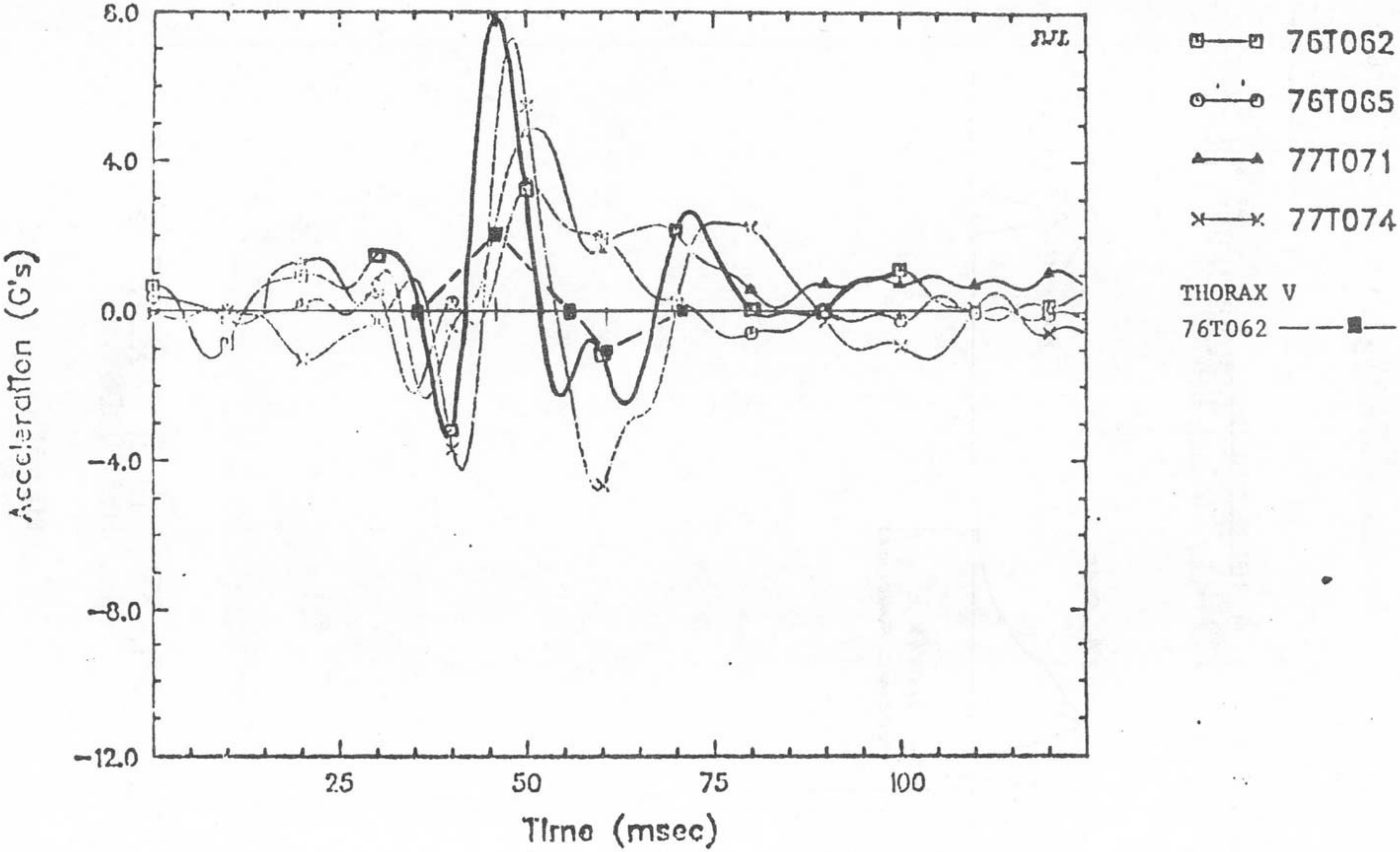

T—12 I—S —— Pend. Side Tests

Fig. 30

77T077
5.0G
20 FP.

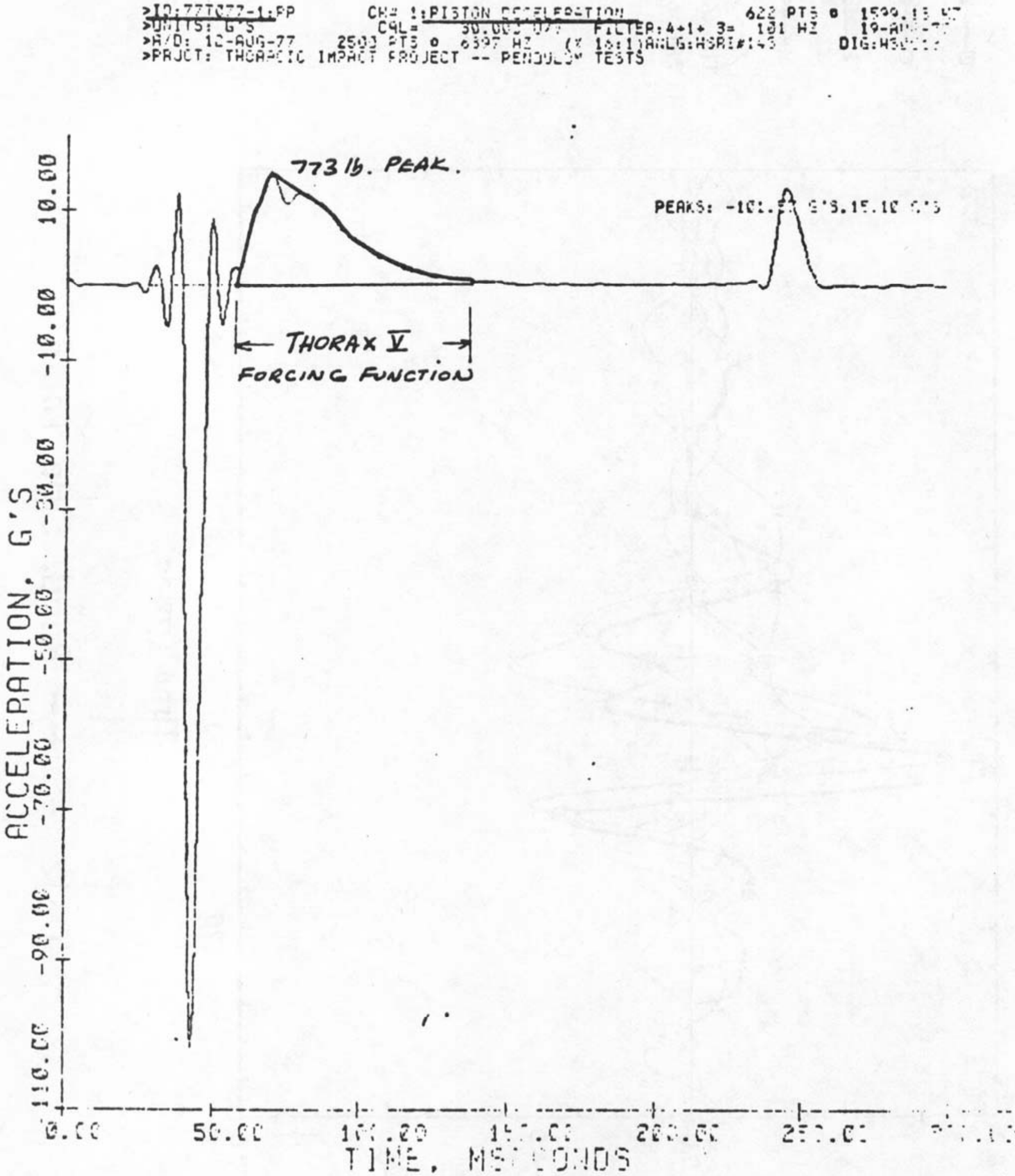

Fig. 31

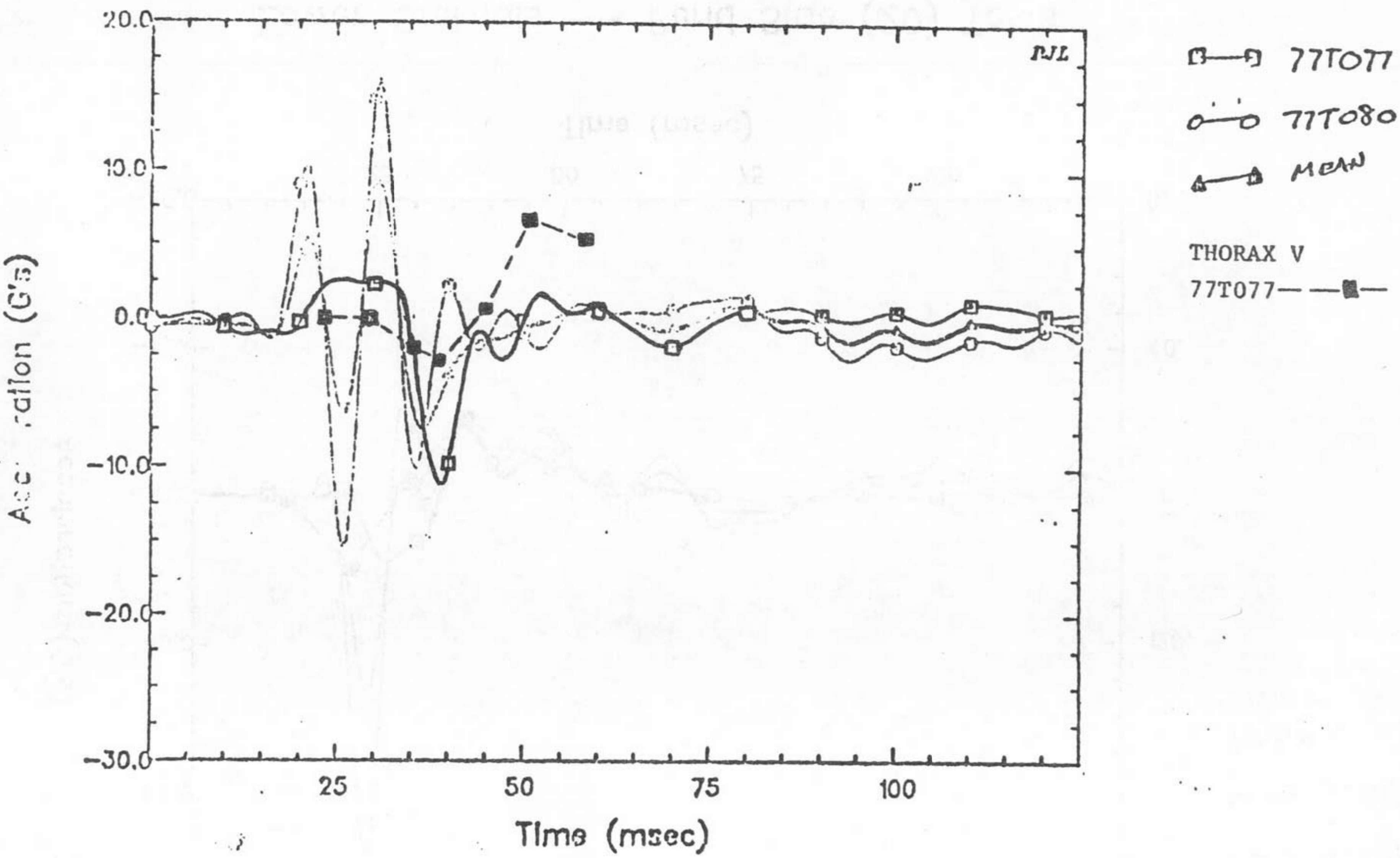

Upper Sternals -- Pend Side (20) Tests

Fig. 32

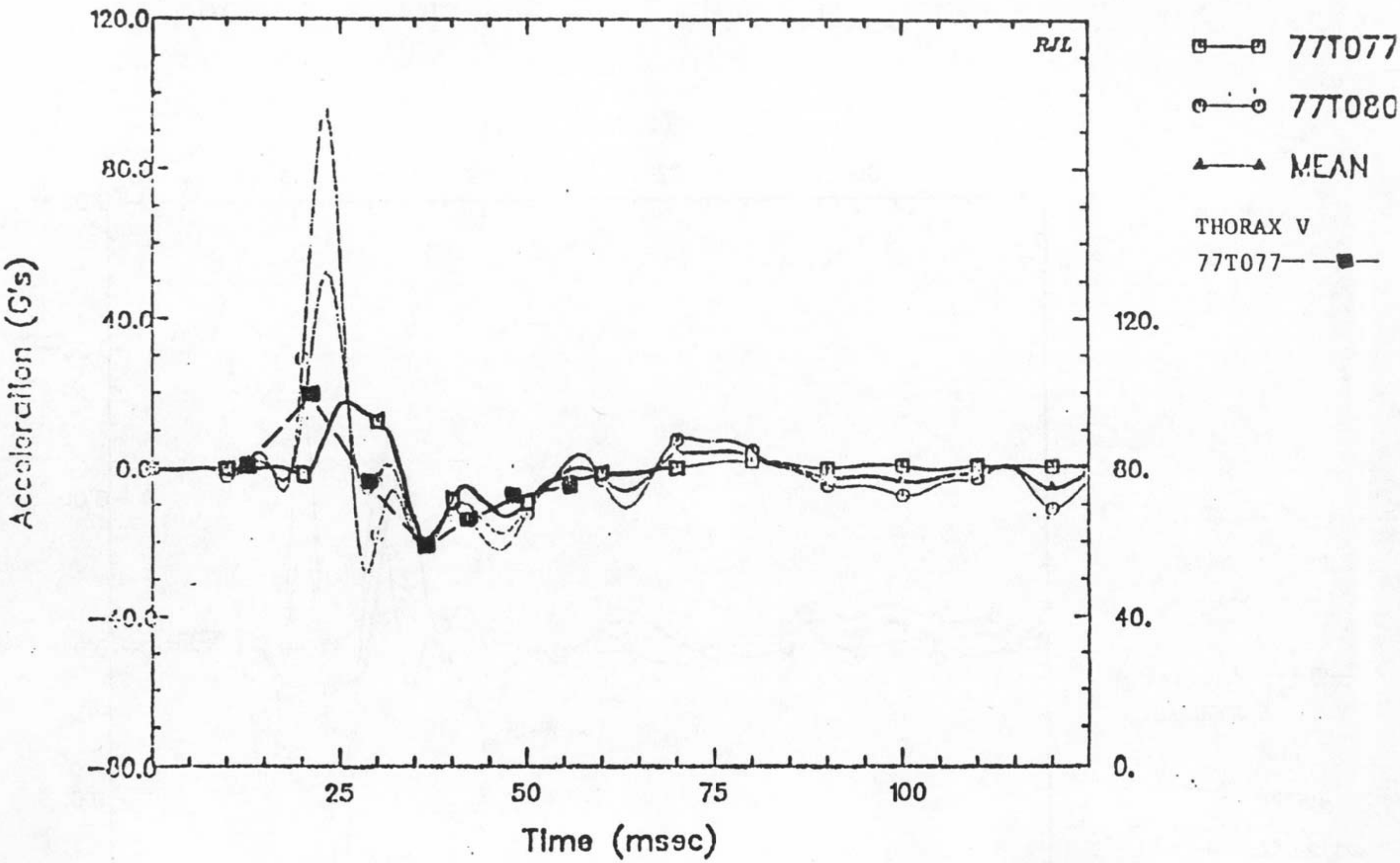

Lower Sternals — Pend Side (20) Tests

Fig. 33

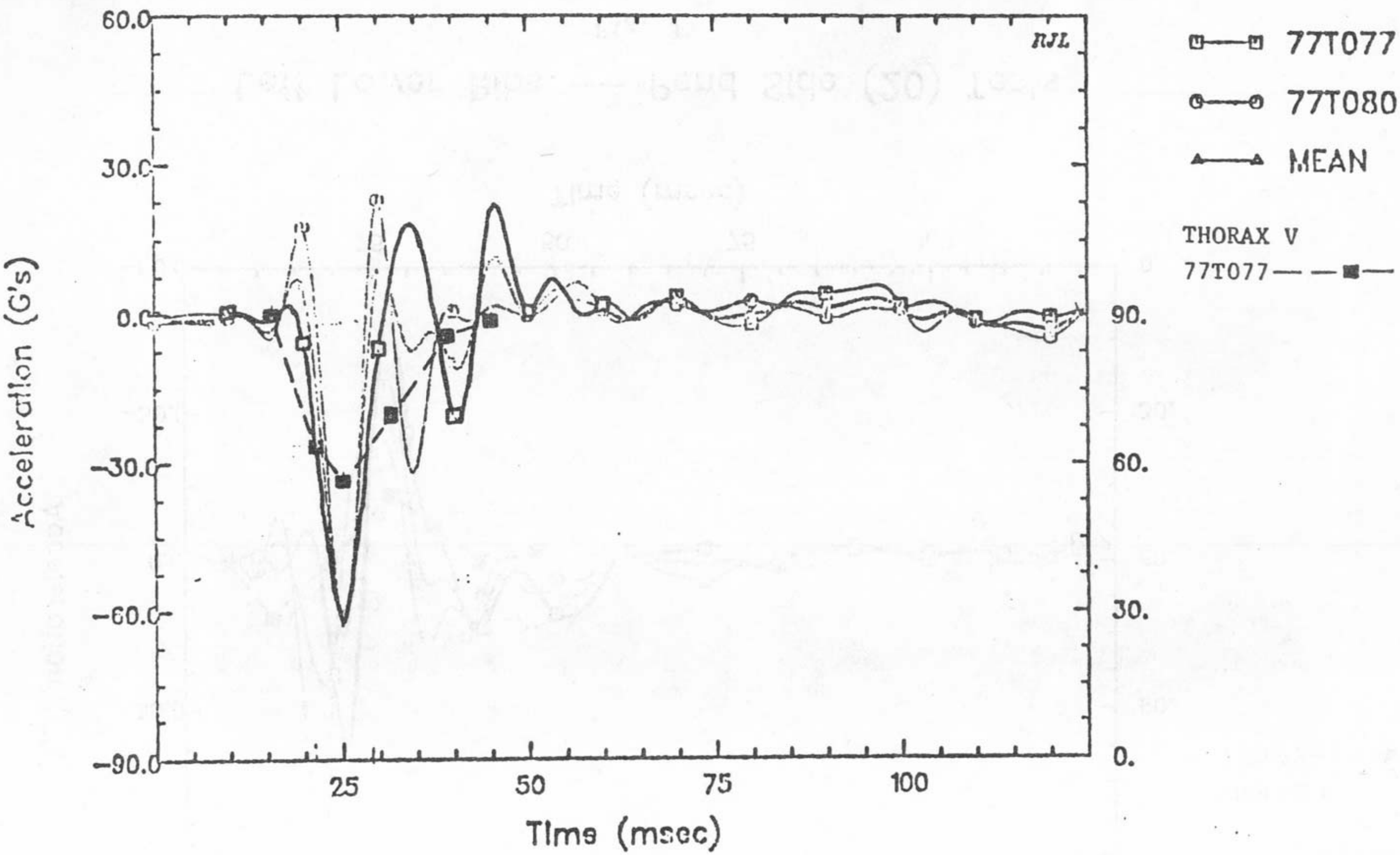

Left Upper Ribs -- Pend Side (20) Tests

Fig. 34

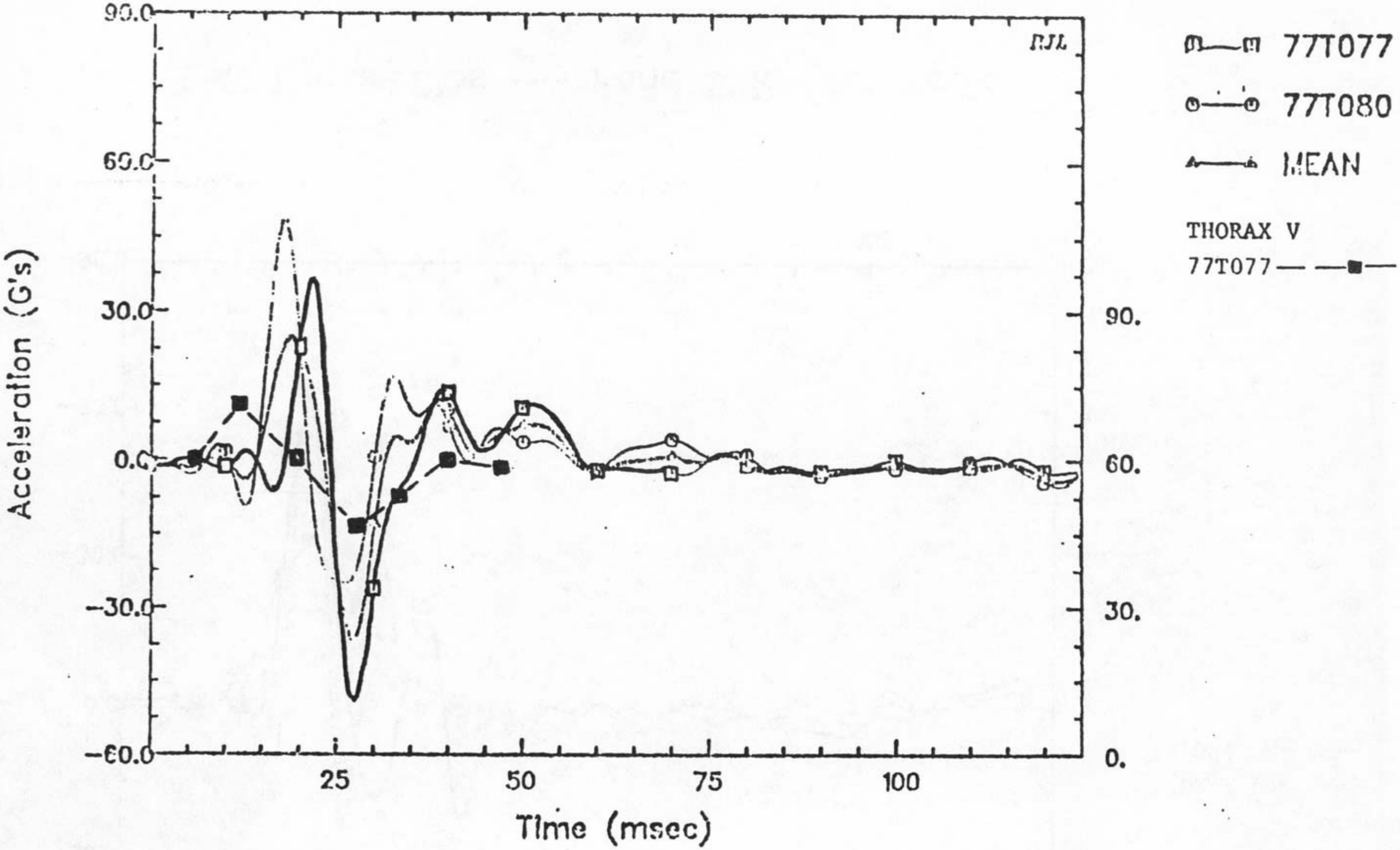

Left Lower Ribs -- Pend Side (20) Tests

Fig. 35

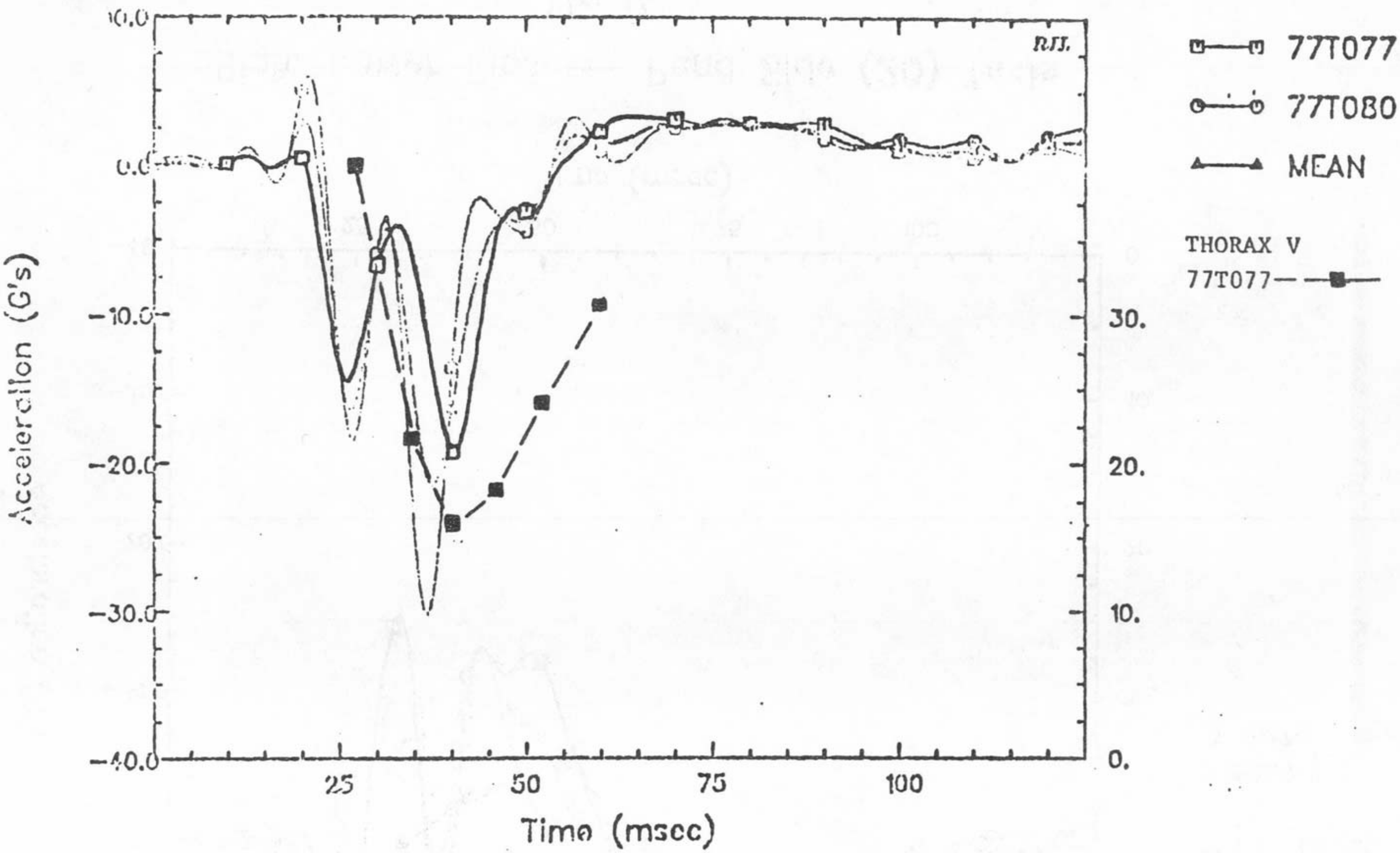

Right Upper Ribs -- Pend Side (20) Tests

Fig. 36

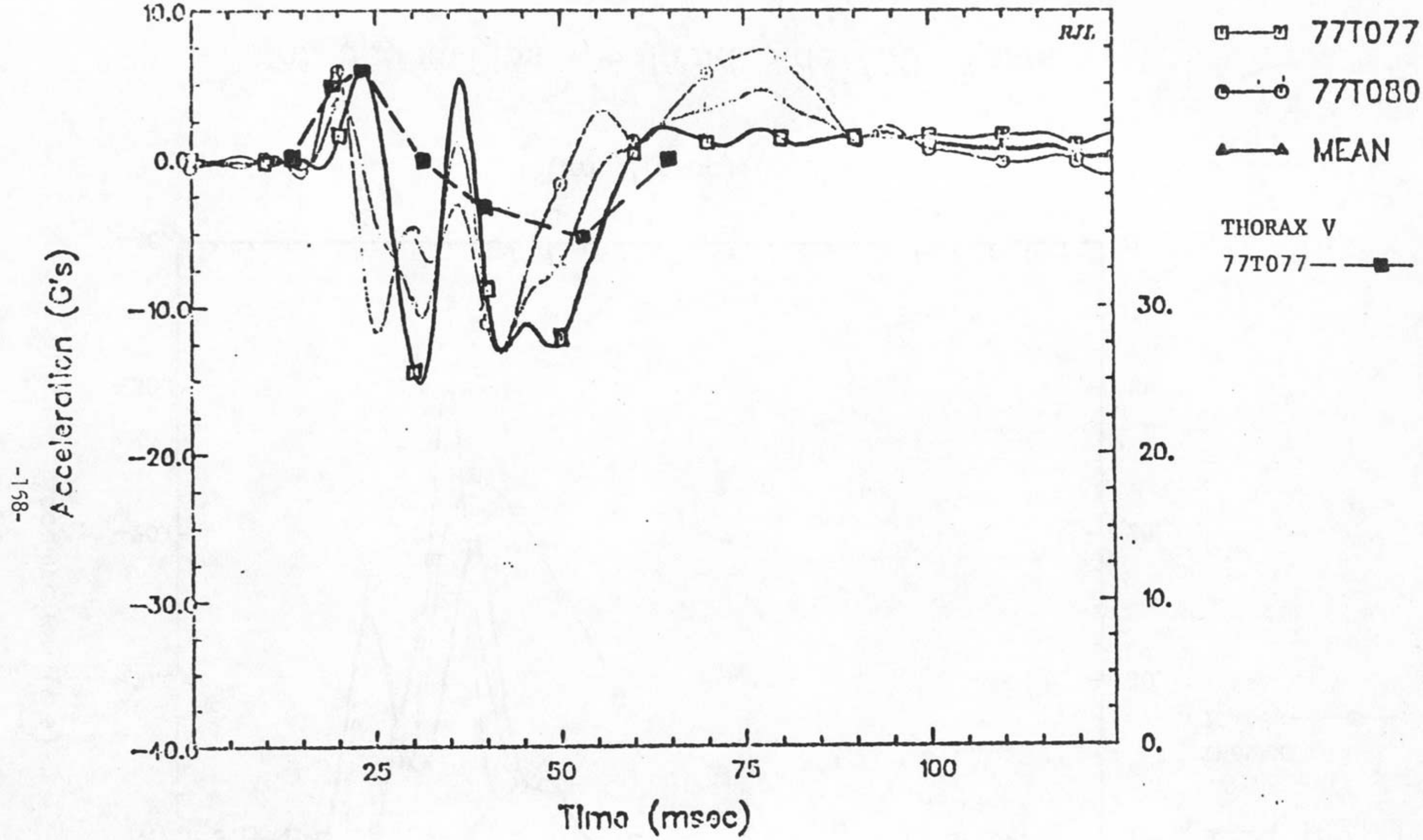

Right Lower Ribs -- Pend Side (20) Tests

Fig. 37

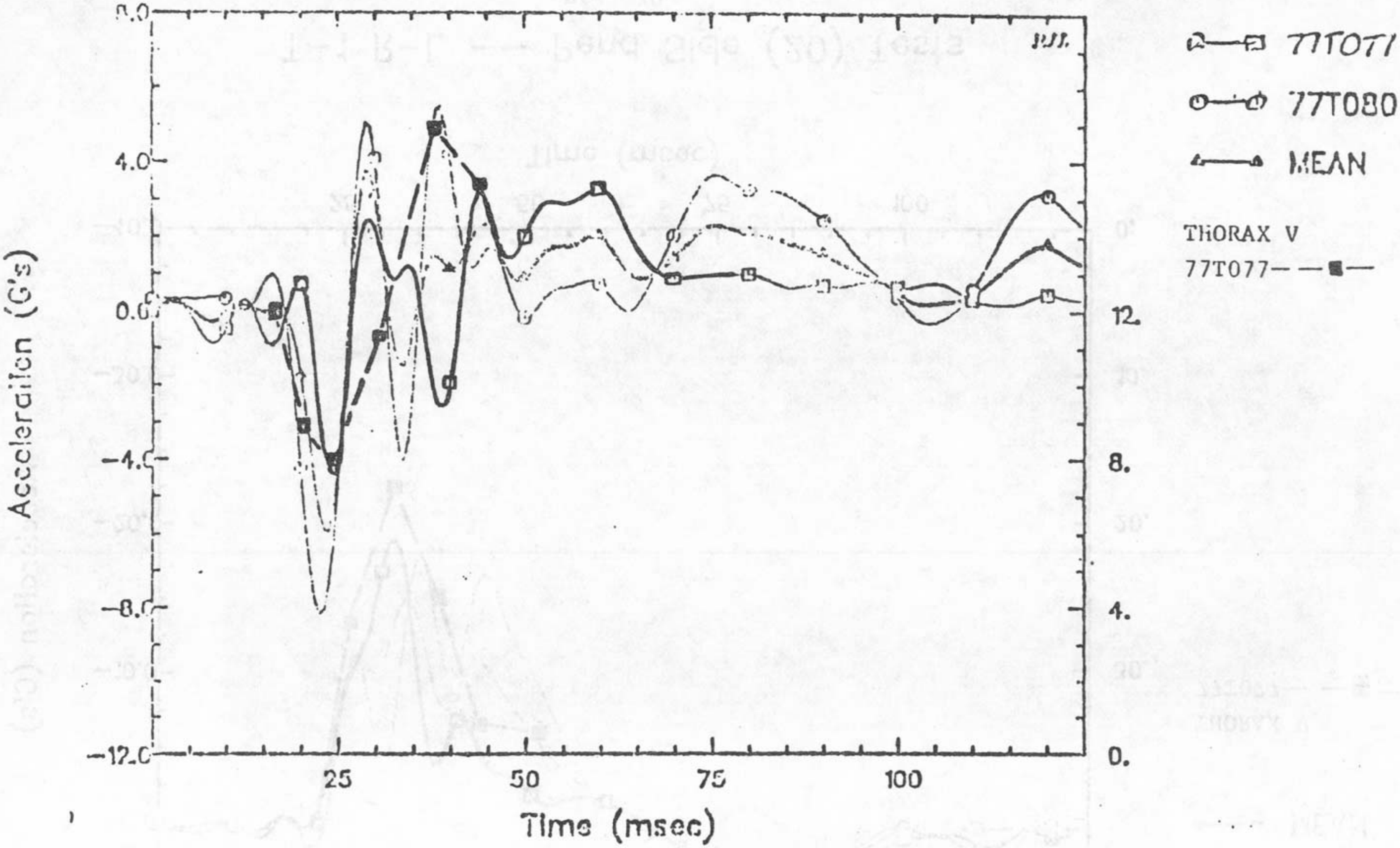

T-1 P-A --- Pend Side (20) Tests

Fig. 38

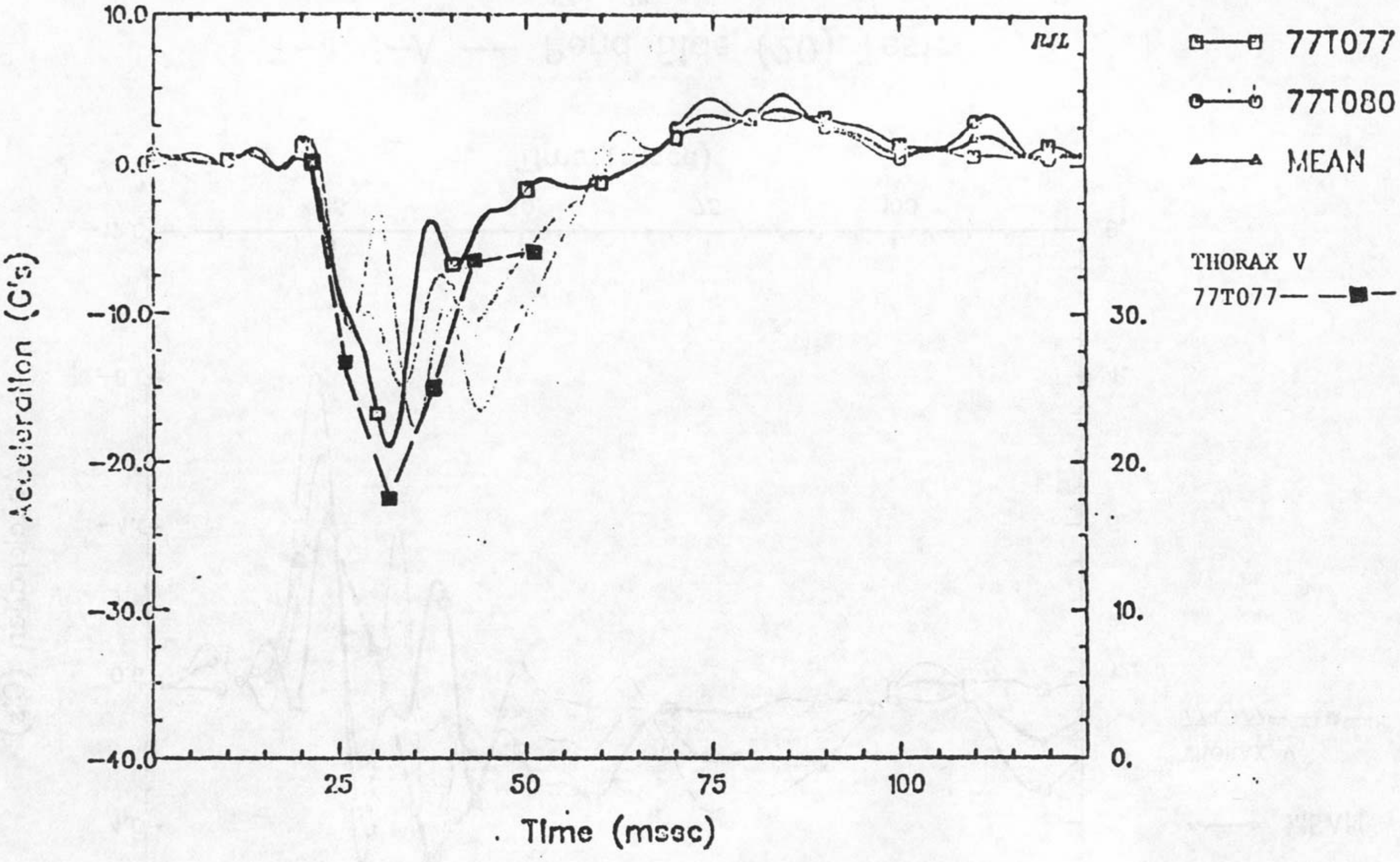

T-1 R-L --- Pend Side (20) Tests

Fig. 39

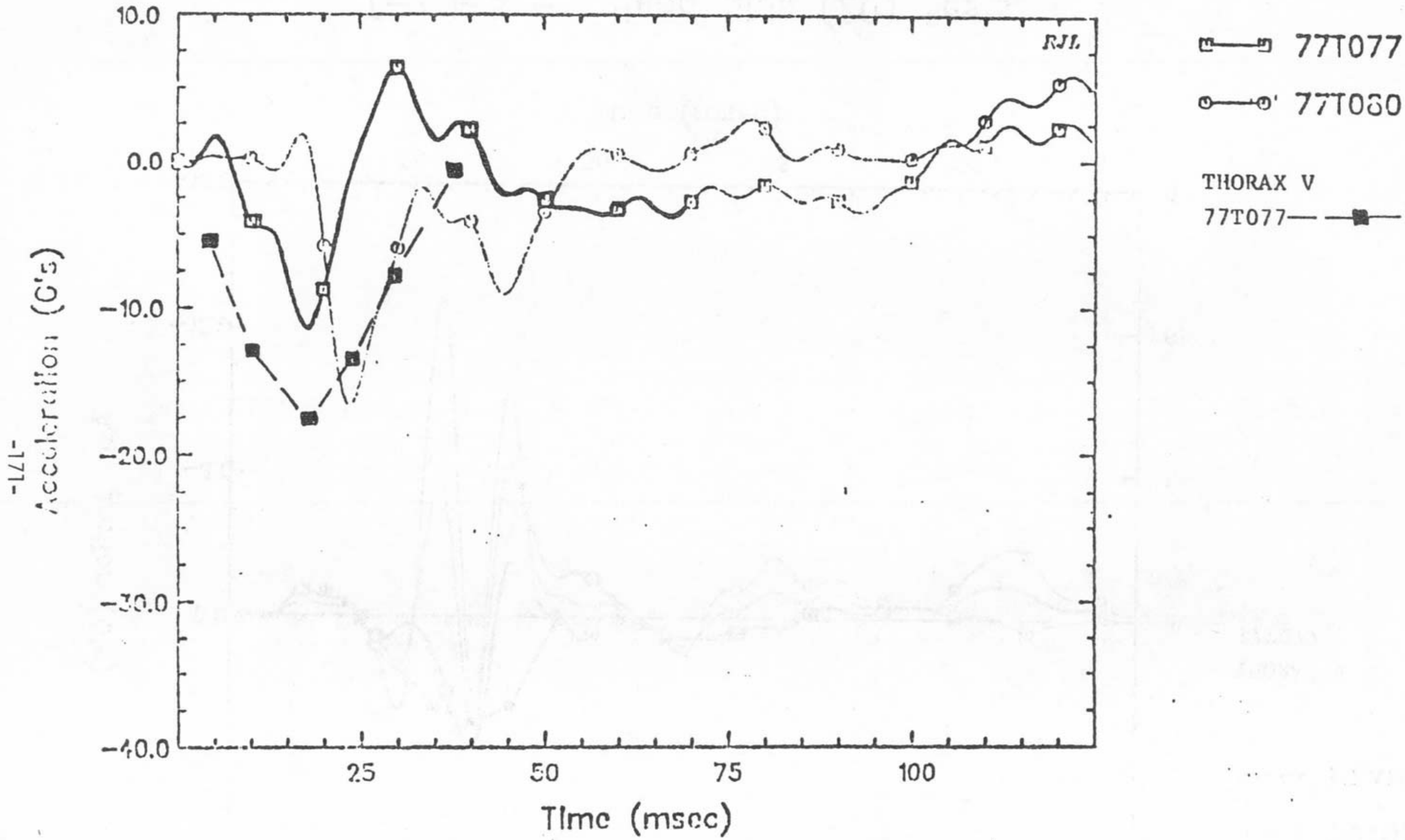

T-12 R-L--PEND SIDE (20) TEST

Fig. 40

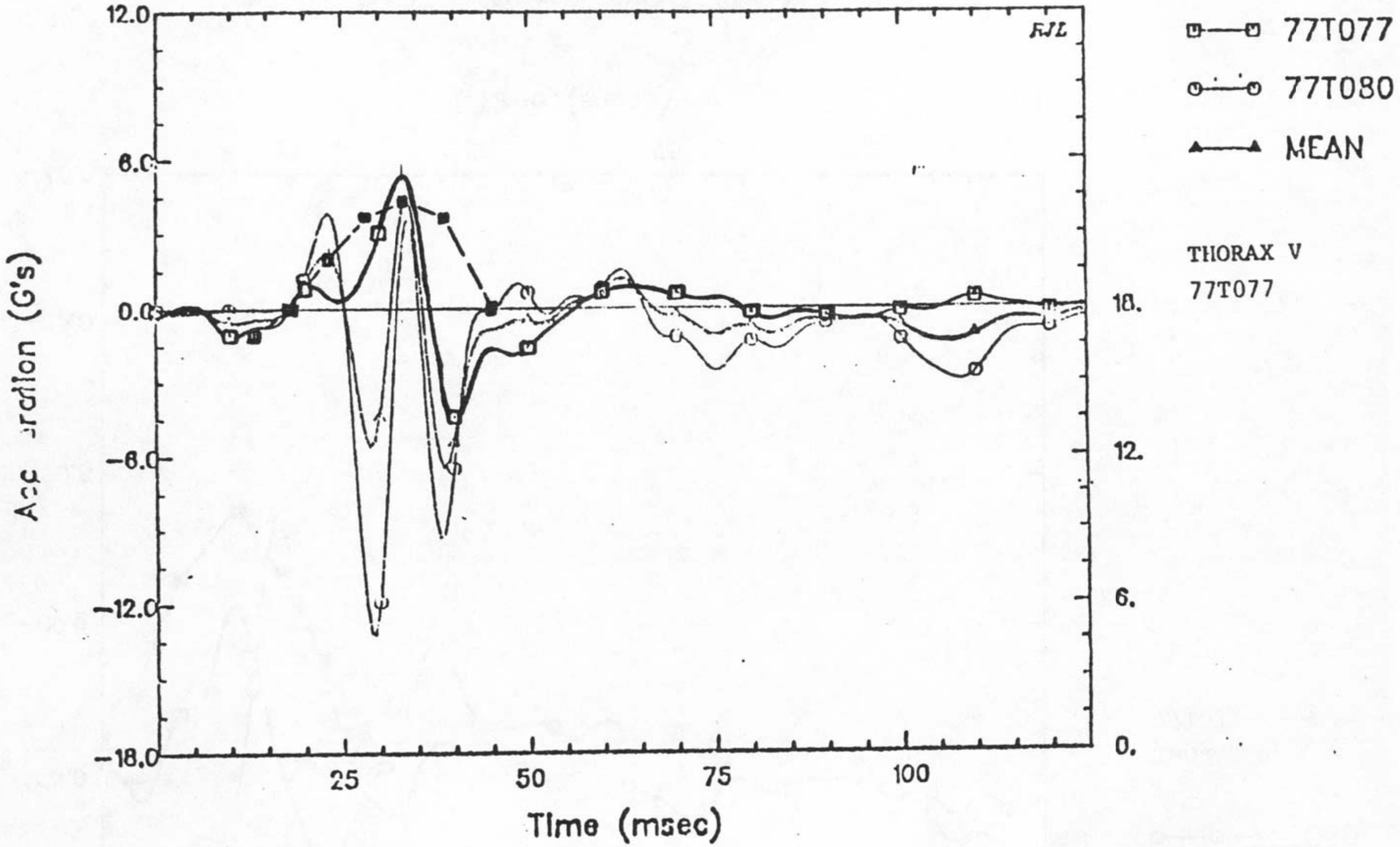

T-1 I-S — Pend Side (20) Tests

Fig. 41

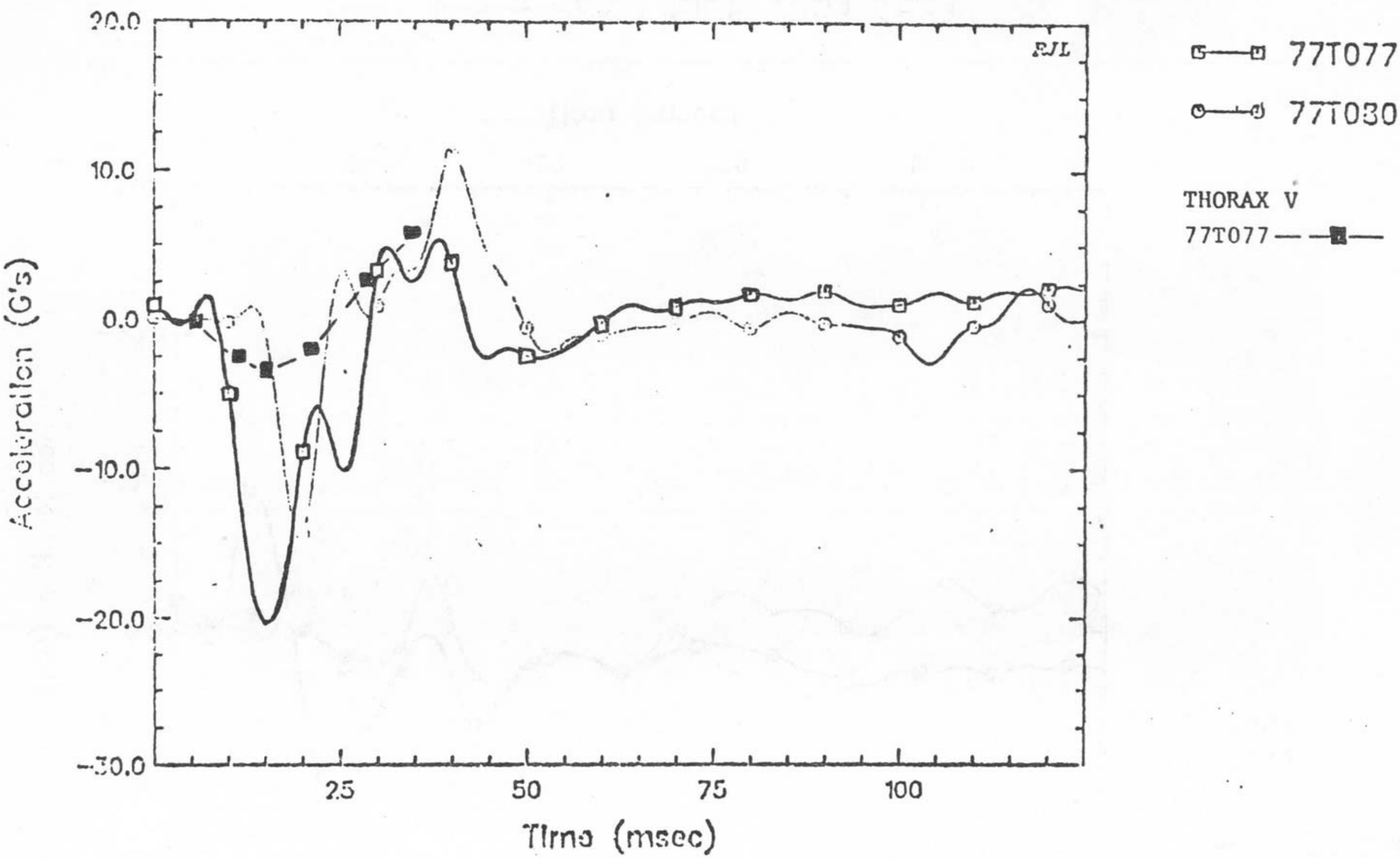

T-12 P-A--PEND SIDE (20) TEST

Fig. 42

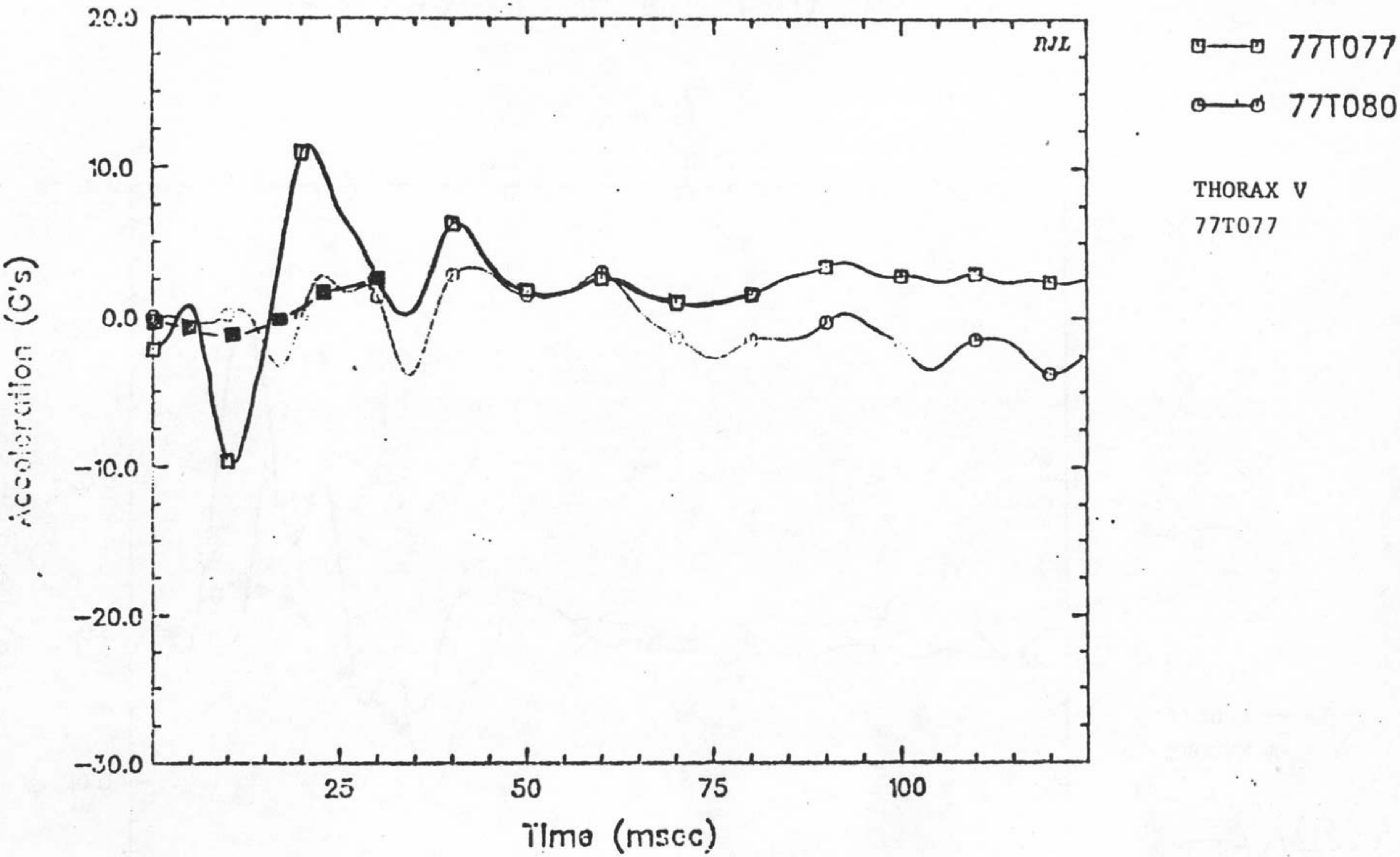

T-12 I-S--PEND SIDE (20) TEST

Fig. 43